Task-Specific Ionic Liquid for Solubilizing Metal Oxides

Peter Nockemann,[†] Ben Thijs,[†] Stijn Pittois,[‡] Jan Thoen,[‡] Christ Glorieux,[‡] Kristof Van Hecke,[§] Luc Van Meervelt,[§] Barbara Kirchner,[||] and Koen Binnemans*,[†]

Laboratories of Coordination Chemistry and Biomolecular Architecture, Department of Chemistry, Katholieke Universiteit Leuven, Celestijnenlaan 200F, and Laboratory of Acoustics and Thermal Physics, Department of Physics and Astronomy, Katholieke Universiteit Leuven, Celestijnenlaan 200D, B-3001 Leuven, Belgium, and Institut für Physikalische und Theoretische Chemie, Universität Bonn, Wegelerstrasse 12, D-53115 Bonn, Germany

Received: July 8, 2006; In Final Form: August 14, 2006

Protonated betaine bis(trifluoromethylsulfonyl)imide is an ionic liquid with the ability to dissolve large quantities of metal oxides. This metal-solubilizing power is selective. Soluble are oxides of the trivalent rare earths, uranium(VI) oxide, zinc(II) oxide, cadmium(II) oxide, mercury(II) oxide, nickel(II) oxide, copper(II) oxide, palladium(II) oxide, lead(II) oxide, manganese(II) oxide, and silver(I) oxide. Insoluble or very poorly soluble are iron(III), manganese(IV), and cobalt oxides, as well as aluminum oxide and silicon dioxide. The metals can be stripped from the ionic liquid by treatment of the ionic liquid with an acidic aqueous solution. After transfer of the metal ions to the aqueous phase, the ionic liquid can be recycled for reuse. Betainium bis(trifluoromethylsulfonyl)imide forms one phase with water at high temperatures, whereas phase separation occurs below 55.5 °C (temperature switch behavior). The mixtures of the ionic liquid with water also show a pH-dependent phase behavior: two phases occur at low pH, whereas one phase is present under neutral or alkaline conditions. The structures, the energetics, and the charge distribution of the betaine cation and the bis(trifluoromethylsulfonyl)imide anion, as well as the cation−anion pairs, were studied by density functional theory calculations.

Introduction

There is much current interest in ionic liquids. These compounds are examples of molten salts that are liquid at temperatures below 100 °C or sometimes even at room temperature.[1−12] The much lower melting points of ionic liquids compared to inorganic salts can be partially attributed to the bulky cationic groups, i.e., low charge density and incompatibility of Coulombic attraction forces with steric hindrance. Ionic liquids have very low vapor pressures, although it was recently shown that they are distillable.[13,14] Therefore, they do not produce hazardous vapors (in contrast to many conventional organic solvents). Most ionic liquids have high ignition points, and they do not generate explosive air−vapor mixtures. They can act as solvents for chemical reactions, including catalytic reactions.[15−20] Ionic liquids are an interesting reaction medium for the synthesis of unusual inorganic compounds.[21−24] They find use in electrochemical applications,[25] for example, as electrolytes in batteries,[26,27] and in photovoltaic devices,[28−30] but also as a medium for electrodeposition[31−34] or electropolishing of metals.[35]

Especially for electrochemical applications and for applications in solvent extraction technology, ionic liquids should have a high solubilizing power for metal salts, including metal oxides. To avoid leaching of the metal catalyst in catalytic reactions, it is of importance to have ionic liquids that can keep metals dissolved in them. A good solubility of metal salts is observed for ionic liquids based on aluminum chloride, such as mixtures of 1-ethyl-3-methylimidazolium chloride and aluminum chloride ($[C_2mim]Cl-AlCl_3$),[36] and mixtures of 1-butylpyridinium chloride and aluminum chloride ($BPC-AlCl_3$).[37] Unfortunately, these systems suffer from extreme water sensitivity; in the presence of water, corrosive hydrogen chloride gas evolves from the ionic liquid. Compounds such as the 1-alkyl-3-methylimidazolium hexafluorophosphates, $[C_n mim][PF_6]$, are room-temperature ionic liquids with a much lower sensitivity toward water.[38,39] Unfortunately, these ionic liquids and related ones such as the 1-alkyl-3-methylimidazolium tetrafluoroborates[40] or the 1-alkyl-3-methylimidazolium bis(trifluoromethylsulfonyl)-imides[41] have a low solubility for metal salts. This can be explained by the weakly coordinating properties of the constituting anions and cations, so that the solvation energy is not high enough to break the binding interactions between the ions or molecules of the metal-containing compounds in the solid state.

To overcome the problems with the solubility of metal salts, researchers are developing so-called *task-specific ionic liquids* (TSILs), which are ionic liquids with a functional group covalently tethered to the cationic or anionic part.[42,43] When the functional group has the ability to coordinate to the metal ion (preferably as a bidentate or a polydentate ligand), it is easier to dissolve metal oxides or metal salts into the ionic liquid. As a rule, these task-specific ionic liquids are not used as single-component ionic liquids, but they are mixed with more conventional ionic liquids. A rationale to use mixtures rather than pure task-specific ionic liquids is that the task-specific ionic liquids often have a higher melting point and a higher viscosity than conventional ionic liquids. Moreover, the conventional ionic liquids are in general much cheaper than the task-specific ionic

* Author to whom correspondence should be addressed. E-mail: Koen.Binnemans@chem.kuleuven.be.
[†] Laboratory of Coordination Chemistry, Department of Chemistry, Katholieke Universiteit Leuven.
[‡] Department of Physics and Astronomy, Katholieke Universiteit Leuven.
[§] Laboratory of Biomolecular Architecture, Department of Chemistry, Katholieke Universiteit Leuven.
[||] Universität Bonn.

10.1021/jp0642995 CCC: $33.50
Published on Web 09/21/2006

liquids. An example of a task-specific ionic liquid is an imidazolium salt incorporating a thiourea moiety, which has been used for the extraction of mercury(II) and cadmium(II) from an aqueous phase.[44] Task-specific ionic liquids with appended tertiary phosphine groups have been used to immobilize rhodium(I) organometallic catalysts in [C_4mim]-[PF_6].[45,46]

The major drawback of these task-specific ionic liquids is that they are often only accessible after a multistep synthetic procedure. The time-consuming preparation of these ionic liquids restricts their use in large-scale industrial applications. Therefore, the development of task-specific ionic liquids that can readily be prepared from cheap raw materials is an important research target. Task-specific ionic liquids that can be prepared from renewable natural resources would even be better. Abbott and co-workers obtained ionic liquids by mixing choline chloride with hydrated transition-metal salts,[47] or with anhydrous zinc(II) chloride or tin(II) chloride.[48,49] The same group also prepared ionic liquids by mixing choline chloride with urea in a 1:2 molar ratio.[50] These mixtures of choline chloride and urea are called *deep eutectic solvents*. They can dissolve different types of metal oxides as well as metal salts, but the solubility of the metal salts in these ionic-liquid-like mixtures is in general less than 1 wt %.[51] A recent study showed that mixtures of choline chloride with malonic acid can dissolve larger quantities of metal oxides.[52] *Choline chloride* (also known as 2-hydroxyethyltrimethylammonium chloride or vitamin B4) is a cheap commodity chemical that is produced annually on a multiton scale. Its main use is as an animal feed additive. Choline chloride itself is a solid with a high melting point (mp 298−304 °C). Although ionic liquids based on choline chloride have the advantages of being cheap, they are all hydrophilic and miscible with aqueous solvents. This is a problem for applications such as the extraction of metal ions from an aqueous phase or the electrodeposition of reactive metals (e.g., aluminum, magnesium, tantalum, and the rare earths).

In a search for cheap and easily accessible cationic building blocks for ionic liquid alternatives for choline, we turned our attention to betaine. Betaine is a trivial name for 1-carboxy-*N*,*N*,*N*-trimethylmethanaminium hydroxide. It is also known as *N*,*N*,*N*-trimethylglycine, *N*-trimethylglycine, or trimethylglycine. Betaine has a zwitterionic structure, and it is thus an inner salt. The difference between the choline and the betaine cation is that in the betaine cation the hydroxyl group is replaced by a carboxylic acid group. In fact, betaine is a metabolite that is formed by oxidation of choline.[53] The carboxylate group of betaine is a much better coordinating group toward metal ions than the aliphatic alcohol function of choline. The most important form of betaine on the market is the hydrochloride salt, betaine hydrochloride. In this paper, we introduce protonated betaine bis(trifluoromethylsulfonyl)imide, [Hbet][Tf_2N], as a new task-specific ionic liquid for selective solubilization of metal oxides and metal salts (Figure 1). The main physical and structural properties of this compound are presented. The temperature-dependent miscibility of the ionic liquid with water has been studied. Of importance is the formation of a one-phase binary mixture at high temperature and a two-phase binary mixture at ambient temperatures. It will be shown that the phase behavior of [Hbet][Tf_2N]−water mixtures strongly depends on the pH conditions. We have performed density functional theory (DFT) calculations to gain more insight into the essential intermolecular forces. Several conformers were considered. The solubility of different metal oxides and metal salts has been studied into detail, including the crystal structures of the copper(II) and dysprosium(III) complexes formed upon dissolution of the corresponding metal oxides in the ionic liquid.

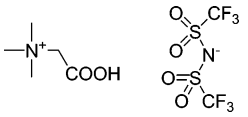

Figure 1. Structure of [Hbet][Tf_2N].

Experimental Section

General Techniques. Elemental analyses (carbon, hydrogen, nitrogen) were made on a CE Instruments EA-1110 elemental analyzer. FTIR spectra were recorded on a Bruker IFS-66 spectrometer. The samples were measured using the KBr pellet method or as a thin film between KBr windows. ^{1}H NMR spectra were recorded on a Bruker Avance 300 spectrometer (operating at 300 MHz). The water content of the ionic liquids was determined by a coulometric Karl Fischer titrator (Mettler Toledo, model DL39). The viscosity of the ionic liquids was measured by the falling ball method (Gilmont Instruments). Differential scanning calorimetry (DSC) measurements were made on a Mettler-Toledo DSC822e module (scan rate of 10 °C min^{-1} under helium flow). Betaine hydrochloride and betaine were purchased from Acros Organics, and lithium bis(trifluoromethylsulfonyl)imide was purchased from IoLiTec. All chemicals were used as received, without any additional purification step.

Quantum Chemical Methodology. DFT calculations with the density functional B3LYP[54,55] were performed for isolated complexes using Turbomole.[56] The TZVP basis set from the Turbomole library is employed throughout.[57] All interaction energies are calculated with the supermolecular ansatz. All the interaction energies of the isolated cation and anion are counterpoise-corrected (CP) using the procedure of Boys and Bernardi.[58,59] However, counterpoise corrections have not been included during the structure optimization. Moreover, second-order Møller−Plesset (MP2) perturbation theory, in combination with the *resolution of the identity technique* (RI), has been applied.[60,61] Atomic charges with multicenter corrections from the shared-electron population analysis are also given in some sections.[62] We obtained the dihedral angles from the figures generated by the visualization program Molden.[63] Within this program, the dihedral angle is defined at 180° as *trans*. Negative values point in counterclockwise directions. Structures were also visualized with Molden[63] and VMD.[64] The electrostatic potential was obtained with the program package Gaussview[65] from a B3LYP/6-31G++(d,p) single-point calculation at the B3LYP/TZVP level or experimental structures. The calculation of the electron localization function was carried out with the CPMD code.[66] The gradient-corrected local density functionals for exchange BLYP[67,68] were used throughout, and the Kohn−Sham orbitals were expanded in a plane wave basis with a kinetic energy cutoff of 70 Ry. In general, norm-conserving pseudopotentials of the Troullier−Martins type were taken.[69] The pseudopotentials were applied in the Kleinman-Bylander representation with the highest angular momentum as the local potential.[70] The shared electron number (SEN) analysis was done as developed by Davidson and Roby (Davidson−Roby population analysis).[71,72]

Photopyroelectric Measurements. The setup for the photopyroelectric measurements is described in detail elsewhere.[73−75] The upper and lower parts of the sample were locally sandwiched between a 216 μm $LiTaO_3$ pyroelectric transducer with chromium−gold electrodes and a 25 mm gold-coated copper backing cylinder. Sample thicknesses were, respectively, around

200 and 180 μm for the upper and the lower phases, and a slight temperature dependence (typically a 10% change over 40 °C due to thermal expansion) was calibrated. The other side of the transducer was in contact with air and was illuminated (and thus heated, via the process of optical absorption of the light at the electrode) by a periodically intensity modulated light-emitting diode (LED).

The purpose of the dual-sensor configuration is to enable simultaneous measurements of the upper and the lower coexisting phases upon phase separation. The measuring cell is incorporated into a temperature-controlled stage with a temperature stability better than 1 mK, which also allows temperature ramping as low as 0.2 mK/min. Since measurements are performed at varying temperatures within the sample in a closed cell and with a small volume of air and sample vapor, the pressure changes differently on the dry and wet sides of the sensors, which may cause it to bend, leading to a small change of the sample thickness. To avoid this, the top of the sample volume and the dry air volume on the other side of the sensors are connected by a tube-membrane system. The movable but sealing flexible membrane prevents sample vapor from condensing or contaminating the dry side of the sensors.

During the temperature scans, both sensors are irradiated with near-infrared radiation, intensity modulated at two different frequencies simultaneously. From the theory of photothermal signals in a 1D configuration[75] (the lateral dimensions of the sample, transducers, and backings were around 18 mm, which is significantly larger than the thermal diffusion lengths in the different layers), one finds that, by properly choosing the modulation frequency, the signal of the transducer, which is proportional to its integrated temperature variations, renders information on the thermal effusivity or on the thermal conductivity of the sample. One frequency is very low (0.36 Hz) and is in the thermal conductivity mode. The other frequency is higher (3 Hz) and is in the effusivity mode. The response of every sensor is measured using two lock-in amplifiers (Stanford Research Systems SR85O and SR830), one for every frequency. The amplitude and the phase of the signal of these four lock-in amplifiers are logged every 20 s. A measurement is performed on a reference sample with known thermal conductivity and effusivity to determine the change of sample thickness as a function of the temperature, which is caused by the thermal expansion of the cell materials.

X-ray Crystallography. Single crystals of [Hbet][Tf_2N] were formed by spontaneous crystallization of the melt after it stood for 5 days at room temperature. Single crystals of [(Hbet)$_3$(bet)][Tf_2N]$_3$ were obtained from a mixture of [Hbet][Tf_2N] and [C_4mim][Tf_2N]. The compounds [Cu(bet)$_4$(H_2O)$_2$][Cu$_2$(bet)$_4$(H_2O)$_2$][Tf_2N]$_6$ and [Dy_2(bet)$_8$(H_2O)$_4$][Tf_2N]$_6$ gave single crystals suitable for X-ray diffraction studies by crystallization from an aqueous solution which was left to evaporate at room temperature.

X-ray intensity data were collected on a SMART 6000 diffractometer equipped with a CCD detector using Cu Kα radiation (λ = 1.54178 Å). The images were interpreted and integrated with the program SAINT from Bruker.[76] All four structures were solved by direct methods and refined by full-matrix least-squares on F^2 using the SHELXTL program package.[77] Non-hydrogen atoms were anisotropically refined and the hydrogen atoms in the riding mode with isotropic temperature factors fixed at 1.2 times the U(eq) of the parent atoms (1.5 times for methyl groups). CCDC 616791, CCDC 616792, CCDC 616793, and CCDC 616794 contain the supplementary crystallographic data for this paper and can be obtained free of charge via www.ccdc.cam.ac.uk/conts/retrieving.html (or from the Cambridge Crystallographic Data Centre, 12 Union Rd., Cambridge CB2 1EZ, U.K., fax +44-1223-336033, e-mail deposit@ccdc.cam.ac.uk).

Data for [Hbet][Tf_2N]: $C_7H_{12}F_6N_2O_6S_2$, M_w = 398.33, orthorhombic, *Pbca* (No. 61), a = 23.4721(8) Å, b = 10.2027(4) Å, c = 25.5957(8) Å, V = 6129.6(4) Å^3, T = 100(2) K, Z = 16, ρ_{calcd} = 1.727 g cm^{-3}, μ(Cu Kα) = 4.107 mm^{-1}, F(000) = 3232, crystal size 0.45 × 0.31 × 0.30 mm, 4884 independent reflections (R_{int} = 0.0695), final R = 0.0400 for 4193 reflections with $I > 2\sigma(I)$, and wR2 = 0.1007 for all data.

Data for [(Hbet)$_3$(bet)][Tf_2N]$_3$: $C_{26}H_{47}F_{18}N_7O_{20}S_6$, M_w = 1312.13, monoclinic, $P2_1/c$ (No. 14), a = 8.2731(6) Å, b = 13.0086(10) Å, c = 24.9865(18) Å, β = 95.181(3)°, V = 2678.1(3) Å^3, T = 293(2) K, Z = 2, ρ_{calcd} = 1.627 g cm^{-3}, μ(Cu Kα) = 3.618 mm^{-1}, F(000) = 1340, crystal size 0.5 × 0.3 × 0.15 mm, 4986 independent reflections (R_{int} = 0.1356), final R = 0.0631 for 2532 reflections with $I > 2\sigma(I)$, and wR2 = 0.1674 for all data.

Data for [Cu(bet)$_4$(H_2O)$_2$][Cu$_2$(bet)$_4$(H_2O)$_2$][Tf_2N]$_6$: $C_{52}H_{88}Cu_3F_{36}N_{14}O_{44}S_{12}$, M_w = 2872.85, monoclinic, $P2_1/n$ (No. 14), a = 15.2183(2) Å, b = 26.1383(3) Å, c = 15.6211(2) Å, β = 117.5540(10)°, V = 5508.97(13) Å^3, T = 100(2) K, Z = 2, ρ_{calcd} = 1.732 g cm^{-3}, μ(Cu Kα) = 4.157 mm^{-1}, F(000) = 2906, crystal size 0.4 × 0.25 × 0.2 mm, 10341 independent reflections (R_{int} = 0.0589), final R = 0.0577 for 9391 reflections with $I > 2\sigma(I)$, and wR2 = 0.1661 for all data.

Data for [Dy_2(bet)$_8$(H_2O)$_4$][Tf_2N]$_6$: $C_{52}H_{88}Dy_2F_{36}N_{14}O_{44}S_{12}$, M_w = 3007.20, triclinic, $P\bar{1}$ (No. 2), a = 14.5423(4) Å, b = 14.5866(3) Å, c = 15.0399(4) Å, α = 82.522(2)°, β = 65.9010(10)°, γ = 71.8490(10)°, V = 2767.31(12) Å^3, T = 100(2) K, Z = 1, ρ_{calcd} = 1.804 g cm^{-3}, μ(Cu Kα) = 10.606 mm^{-1}, F(000) = 1498, crystal size 0.35 × 0.25 × 0.15 mm, 10085 independent reflections (R_{int} = 0.0435), final R = 0.0381 for 9276 reflections with $I > 2\sigma(I)$, and wR2 = 0.0945 for all data.

Synthesis of Protonated Betaine Bis(trifluoromethylsulfonyl)imide. A solution of betaine hydrochloride (1 mol, 153.61 g) in 250 mL of water was added under stirring to 500 mL of an aqueous solution of lithium bis(trifluoromethylsulfonyl)imide (1 mol, 287.08 g). The mixture was stirred for 1 h at room temperature. The aqueous phase separated from the ionic liquid. After separation of the phases, the ionic liquid phase was washed three times with small amounts of water until no chloride impurities could be detected by the silver nitrate test. The ionic liquid was evaporated to dryness at 120 °C in vacuo on a rotary evaporator. A water content of 35 ppm was determined by coulometric Karl Fischer titration. ^{1}H NMR (300 MHz, d_6-DMSO, TMS): δ = 4.27 (s, 2H), 3.19 (s, 3 × CH_3). ^{13}C NMR (d_6-DMSO, TMS): δ = 167.38 (COO), 125.99, 121.75, 117.52, 113.28 (2 × CF_3), 64.06 (N−CH_2), 54.16 (3 × CH_3). Anal. calcd for $C_7H_{12}N_2O_6F_6S_2$ (M_w = 398.302): C, 21.10; H, 3.03; N, 7.03. Found: C, 20.78; H, 3.24; N, 6.85. Mp: 57 °C. Density: 1.531 g cm^{-3} (60 °C).

Nomenclature. We name the ionic liquid presented in Figure 1 as protonated betaine bis(trifluoromethylsulfonyl)imide, [Hbet][Tf_2N]. Here we represent the cation betaine by *Hbet* rather than by *bet*, because in [Hbet][Tf_2N] the carboxylate group is protonated. Protonated betaine is sometimes also named as *betainium*,[78] but this name has not received widespread use.

Results

Synthesis of the Betaine Salts. An aqueous solution of betaine hydrochloride reacts with an aqueous solution of lithium bis(trifluoromethylsulfonyl)imide to form [Hbet][Tf_2N]. The

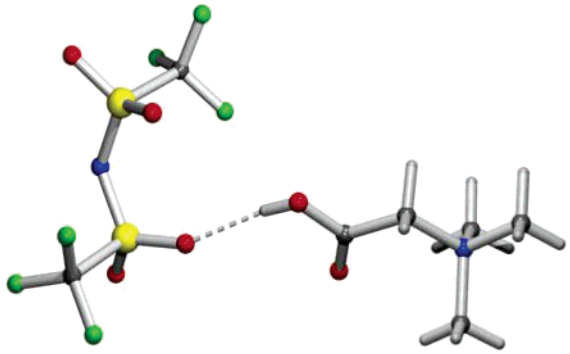

Figure 2. Molecular structure of [Hbet][Tf_2N]. The hydrogen bonding between the $[Hbet]^+$ cation and the $[Tf_2N]^-$ is made visible.

ionic liquid compound easily separates from the aqueous layer. The melting point of [Hbet][Tf_2N] is 57 °C, but the liquid compound can be supercooled to room temperature. [Hbet][Tf_2N] shows a tendency to crystallize rather than to form a glass: after some time (hours to weeks) crystallization occurs. The viscosity of [Hbet][Tf_2N] is 351 cP at 60 °C. [Hbet][Tf_2N] is a hydrophobic ionic liquid at room temperature; after addition of water, two separate phases are formed. [Hbet][Tf_2N] is miscible with ethanol, 1-octanol (and other higher alcohols), benzonitrile, acetonitrile, DMSO, acetic acid, and ethyl acetate, but also with other ionic liquids containing the bis(trifluoromethylsulfonyl)imide anion such as [C_6mim][Tf_2N]. [Hbet][Tf_2N] is immiscible with hexane, heptane, DCM, chloroform, benzene, toluene, and diethyl ether.

All trials to obtain analogues of protonated betaine bis(trifluoromethylsulfonyl) imide with counterions other than bis(trifluoromethylsulfonyl)imide resulted in the formation of solids with a high melting point: (1) protonated betaine hexafluorophosphate, [Hbet][PF_6] (mp 159 °C; this compound has been previously reported[79]); (2) protonated betaine triflate, [Hbet][OTf] (mp 125 °C); (3) protonated betaine pentafluorobenzoate, [Hbet][C_6F_6COO] (mp 144 °C).

Crystal Structures of [Hbet][Tf_2N] and [(Hbet)$_3$(bet)][Tf_2N]$_3$. Two different crystal structures were obtained for protonated betaine bis(trifluoromethylsulfonyl)imide, depending on the crystallization conditions. Crystals of [Hbet][Tf_2N] were formed by spontaneous crystallization of a melt of the protonated betaine bis(trifluoromethylsulfonyl)imide ionic liquid. Crystals of the composition [(Hbet)$_3$(bet)][Tf_2N]$_3$ were formed in a mixture of the ionic liquids betaine bis(trifluoromethylsulfonyl)-imide and 1-butyl-3-methylimidazolium bis(trifluoromethylsulfonyl)imide. The melting point of [Hbet][Tf_2N] crystals is 69 °C, whereas that of [(Hbet)$_3$(bet)][Tf_2N]$_3$ crystals is 70 °C. The formation of anion−cation pairs connected by strong hydrogen bonding was found (with an O−(H)···O distance of 1.89 Å or O···O distance of 2.72 Å) in the crystal structure of [Hbet][Tf_2N]. The proton on the carboxylic group could be found in the difference Fourier map. The molecular structure of a hydrogen-bonded anion−cation pair of [Hbet][Tf_2N] is shown in Figure 2.

The crystal structure of [(Hbet)$_3$(bet)][Tf_2N]$_3$ shows tetrameric units of betaine cations which are connected by strong hydrogen bonding (O−O distances range from 2.45 to 2.64 Å) (Figure 3). The four betaine moieties of the tetrameric unit share only three protons, so one betaine zwitterion is present per tetrameric unit. The asymmetric unit contains two betaine moieties. The proton in the center of the tetrameric unit is disordered between the two positions of the carboxylate groups due to the symmetry center in between (space group $P\bar{1}$). One of the two bis(trifluoromethylsulfonyl)imide anions in the asymmetric unit

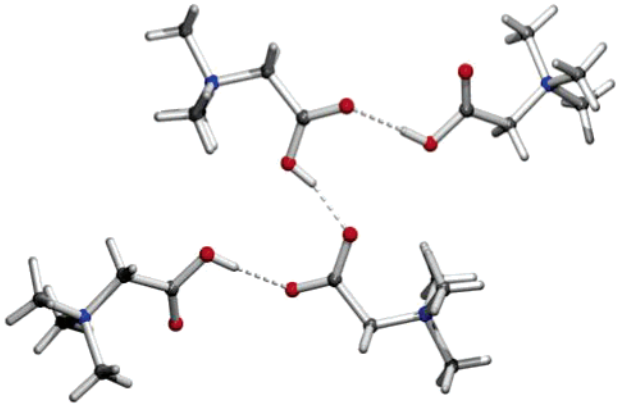

Figure 3. Cationic tetramer $[(Hbet)_3(bet)]^{3+}$ in the molecular structure of [(Hbet)$_3$(bet)][Tf_2N]$_3$.

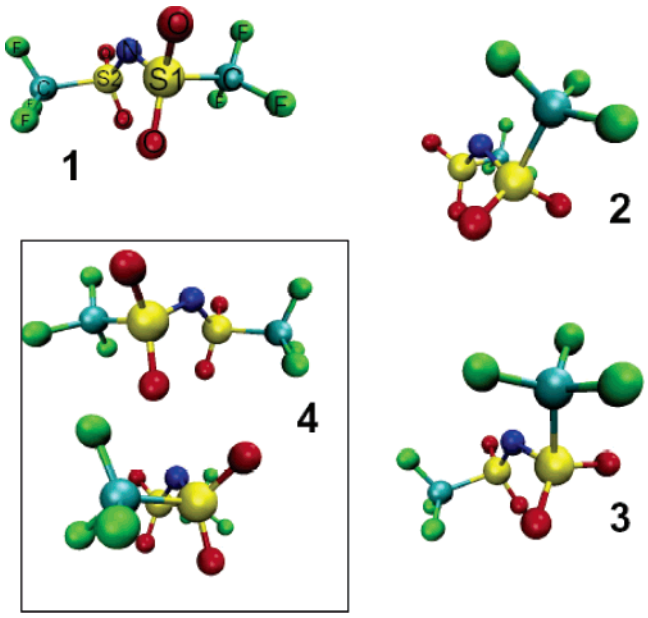

Figure 4. Four local minimum-energy conformations of the anion. In conformer **1**, the atoms have been labeled.

of [(Hbet)$_3$(bet)][Tf_2N]$_3$ is disordered. The bis(trifluoromethylsulfonyl)imide anions surround the tetrameric units outside the range of any further hydrogen bonding.

Quantum Chemical Calculations. The structural properties of isolated clusters consisting of [Hbet][Tf_2N] were obtained by DFT calculations. The calculations were done to learn about the hydrogen bonding in the system, to determine the strength of the cation−anion interaction, and to find out which geometry is more favorable (the most stable conformation in a crystal structure is not necessarily the most stable in an isolated cluster). Finally, we wanted to determine where the negative charges are located on the anion, to get an idea where preferred coordination can occur.

First, the structure of the bis(trifluoromethylsulfonyl)imide anion was optimized. For the structure of the anion, four important local minimum conformers were found (Figure 4). Conformers **1** and **4** are also observed in the experimental crystal structure of [Hbet][Tf_2N]. These two *transoid* conformers can be considered as enantiomers; it is not possible to bring the two anions into accordance by rotating the full molecule, but by mirroring them, it is. Also conformers **2** and **3**, which are *cisoid*, can be considered as enantiomers. Conformers **1** and **3** as well as conformers **2** and **4** can be brought in accordance with each other by the rotation within the anion of one CF_3

TABLE 1: Dihedral Angle *d* (deg), Angle *a* (deg), and Distance *r* (pm) of Different Conformers of the Bis(trifluoromethylsulfonyl)Imide Anion[a]

	1	**2**	**3**	**4**	**1**$_{exptl}$	**4**$_{exptl}$
d(C−S−S−C)	172	79	−77	−170	173	−179
a(S−N−S)	125	123	123	125	124	126
			S1			
r(N−S)	163	163	163	163	157	158
**r*(S−O)	147	148	148	147	143	143
r(S−C)	191	191	191	191	183	183
**r*(C−F)	134	134	134	134	132	133
			S2			
r(N−S)	163	161	161	163	159	157
**r*(S−O)	147	148	148	147	142	143
r(S−C)	191	191	191	191	183	182
**r*(C−F)	134	134	134	134	132	133

[a] For the definition of the atoms, see Figure 4. Since the different oxygen atoms and the fluorine atoms are almost not distinguishable, only one set of S−O and C−F distances is given. The other distances are identical within the error of the calculation method. If, however, exceptional geometrical parameters occur, their values are given in the text. All data are B3LYP/TZVP electronic structure calculations (conformers **1**, **2**, **3**, and **4**), except the experimental structures (**1**$_{exptl}$ and **2**$_{exptl}$).

TABLE 2: Charges (au) on Different Conformers of the Bis(trifluoromethylsulfonyl)Imide Anion from a Multicenter-Corrected SEN Population Analysis[a]

	1	**2**	**3**	**4**	**1**$_{exptl}$	**4**$_{exptl}$
N	−0.642	−0.613	−0.615	−0.642	−0.642	−0.630
			S1			
S	0.877	0.851	0.851	0.879	0.860	0.869
O1	−0.443	−0.447	−0.447	−0.443	−0.456	−0.434
O2	−0.441	−0.440	−0.438	−0.442	−0.435	−0.430
C	0.327	0.342	0.340	0.327	0.315	0.321
F1	−0.174	−0.177	−0.177	−0.175	−0.164	−0.177
F2	−0.168	−0.164	−0.163	−0.168	−0.162	−0.165
F3	−0.158	−0.163	−0.163	−0.157	−0.156	−0.153
			S2			
S	0.877	0.881	0.882	0.878	0.864	0.861
O1	−0.443	−0.468	−0.467	−0.443	−0.433	−0.467
O2	−0.441	−0.434	−0.435	−0.442	−0.422	−0.417
C	0.327	0.328	0.327	0.327	0.319	0.322
F1	−0.175	−0.176	−0.176	−0.174	−0.172	−0.169
F2	−0.168	−0.171	−0.171	−0.168	−0.166	−0.168
F3	−0.157	−0.149	−0.149	−0.157	−0.150	−0.163

[a] For definitions, see Figure 4. Since the oxygen atoms and the fluorine atoms are not comparable, the atoms with the largest absolute charge are ordered first for each conformer at each side, S1 and S2. The data for the experimental structures are obtained from a single-point calculation.

group, being the CF_3 group which points outside the plane (see Figure 4). The optimized structures **1** and **4** as isolated clusters are 2.2 kJ mol^{-1} more stable than the other conformers.

In Table 1, the C−S−S−C dihedral angle *d* (deg), the S−N−S angle *a* (deg), and the distance *r* (pm) of the different conformers of the bis(trifluoromethylsulfonyl)imide anion are listed. The differences in the S−N−S angle for the different conformers are marginal. For the *trans*-conformers **1** and **4**, the S−N−S angle is larger than for both *cis*-conformers **2** and **3**. The dihedral angle can serve as a label for the conformation of the anion. The absolute value of the dihedral angle for the *trans*-conformers exceeds 170°, while the absolute values of the dihedral angles are less than 80° for the *cis*-conformers. From Table 1, one can see that the theoretically calculated values compare well with the experimental data. The largest deviations are observed for the S−C distances. In the crystal structure, these distances are approximately 10 pm shorter than the calculated values. All structures were optimized also with the MP2 method and the TZVP basis set. While the S−O and C−F distances are in the same region as the distances from the structures of the B3LYP optimizations, the N−S distance is reduced by 1 pm (from 163 to 162 pm) and the S−C distance is reduced by 3 pm from 191 pm (B3LYP) to 188 pm (MP2). However, the differences between the crystal structure and the B3LYP-optimized structure can also be due to the fact that the cation in the crystal structure is bound to the anion. It is also evident from Table 1 that the atomic distances in conformers **1** and **4** deviate only little from those of conformers **2** and **3**.

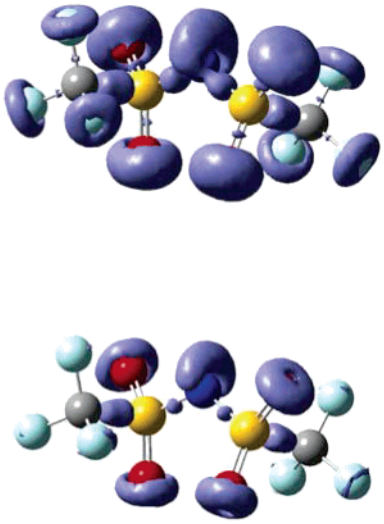

Figure 5. Electron localization function for bis(trifluoromethylsulfonyl)imide conformer **1**: (upper panel) isosurface value 0.85, (lower panel) isosurface value 0.8.

In Table 2, the multicenter-corrected SEN charges of each atom are listed. While most of the negative charge is localized at the nitrogen atom, the carbon and the sulfur atoms are positively charged. The sulfur atoms are by far more positively charged than the carbon atoms. Also the oxygen and fluorine atoms are negatively charged. From this charge analysis it is apparent why any cation would try to interact with the oxygen atom: the oxygen atoms bear a larger negative charge than the fluorine atoms. The nitrogen atom that is by far the most negative center might be sterically hindered to interact with the cation of the ionic liquid. To gain insight into the location of the electron pairs, the *electron localization function* (ELF)[80−82] for conformer **1** was calculated. Figure 5 shows the ELF for two isosurface values, namely, 0.85 and 0.8. Roughly speaking, ELF decomposes the electron density into sections of space which correspond to our intuition of electron pairs. ELF is a function of real space and takes values between 0 and 1. High values of ELF indicate high probabilities of electron pairs, i.e., a higher localization of the electron pairs. Large spheres are observed at the nitrogen typical for two lone pairs (see also the example of the water dimer).[83] Doughnut-shaped spheres are found around the oxygen atoms. Whereas the oxygen atoms are open for an electrophilic attack or coordination from each side, the basin of the central nitrogen atom is only extended at the open side of the S−N−S angle, which means that the electron density is largely localized on this side of the nitrogen atom. Therefore, priorily the oxygen atoms are involved in hydrogen bonding. At the fluorine atoms, the electron pairs are less probable than around the oxygen atoms, which is in accordance with the charge distribution. As a result, the preferred hydrogen-bonding acceptor will again be one of the oxygen

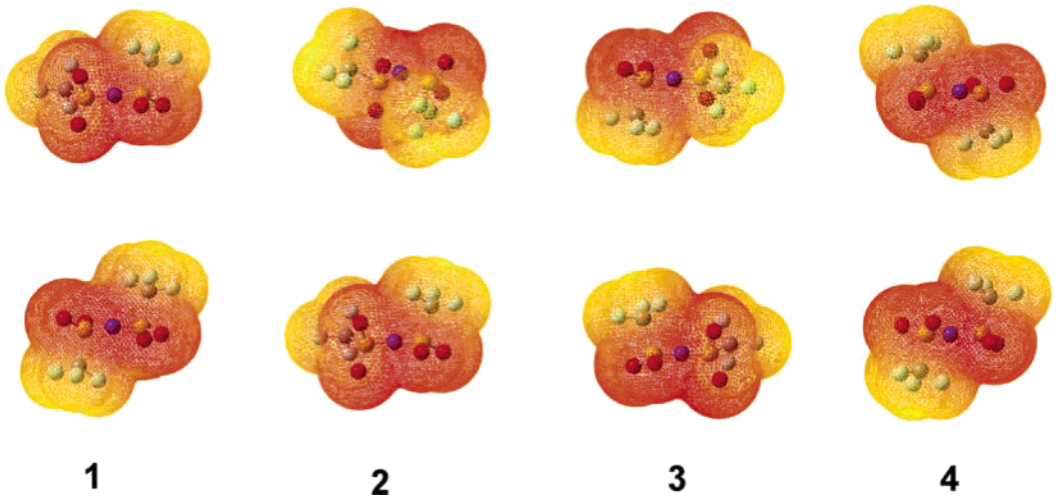

Figure 6. Electron density (0.0004 isosurface value) mapped with electrostatic potential of the bis(trifluoromethylsulfonyl)imide anion. The scale spans from −0.172 (red) to +0.172 (blue). Because of the similarities between **1** and $\mathbf{1}_{exptl}$ as well as between **4** and $\mathbf{4}_{exptl}$, only one from each pair is shown. The upper panel shows the anion with the nitrogen atom pointing out of the plane of the paper. The lower panel depicts the opposite direction.

atoms instead of one of the fluorine atoms, although fluorine is the more electronegative element. The lone pairs at the nitrogen atom enforce the bending of the anions, but the bending is not as large as in the water molecule; the S−N−S angle is between 123° and 126° in the $[Tf_2N]^-$ anion (see Table 1), whereas the H−O−H angle is 109° in water. The larger angle of the anion is due to the fact that the electron pairs repel each other at the two oxygen atoms opposite the nitrogen atom.

The electrostatic potential mapped onto the electron density shows that the regions of red areas that are spread over the density of the anion are larger in conformer **1** than in conformer **4**. In conformers **2** and **3** the nitrogen atom is shielded by one of the CF_3 groups. This again clearly indicates that the oxygen atoms will be preferred as acceptors for hydrogen bonding.

After optimization of the bis(trifluoromethylsulfonyl)imide anion, the protonated betaine cation was optimized. In the crystal structure of [Hbet][Tf_2N], two different protonated betaine cations with very similar structures are present (see above). After optimization by DFT calculations, both conformers **1** and **2** were found to be identical (Figures 4 and 6). The experimental and the calculated distances *r*(OH) (within the alcoholic group) deviate by 13 pm and distances from the alcohol proton to the carbonyl oxygen, *r*(O′H), deviate only by 6 pm from each other. The values obtained after optimizations are similar to the results of Szafran and Koput using a 6-31G(d,p) basis set in combination with HF (95 pm), MP2 (97 pm), and DFT (99 pm).[84] The structure of the carboxylate group is planar, as was expected. Both atoms, the nitrogen and the carbon atom, are very positively charged, but the carbon atom of the carboxylate group is more positively charged than the nitrogen atom (see Table 3). This is the reason the ions in the ion pair will connect in a way that brings the carbon atom closer than the nitrogen atom to the anion. The hydrogen bonding by the carboxylate group is obvious, since the carboxylate proton is very positively polarized. Interaction of the anion at the side of the ammonium group is possible, which can be observed by the dark (blue) areas in the electron density map (Figure 7). This is the reason in the gas phase where no concurrent neighbor ion is present the betaine also interacts with the ammonium group. Glycine betaine and its hydrates were calculated by Shikata.[85] For the unprotonated zwitterion a high dipole moment of 11 D was found by using HF and MP2 calculations with a 6-31G** basis

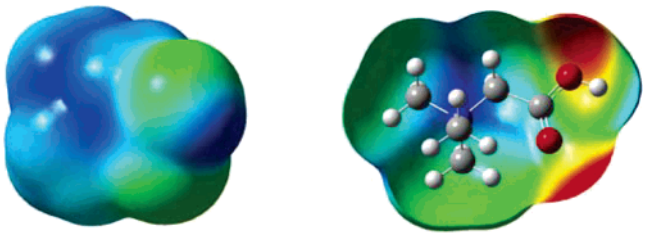

Figure 7. Electron density (0.0004 isosurface value) mapped with the electrostatic potential of the protonated betaine cation. The scale spans the narrow range between 0.1 (red) and 0.184 (blue) to illustrate subtle features.

TABLE 3: Distance *r* (pm) and Charge *q* (au) for the Isolated Protonated Betaine Cation[a]

ion	*r*(OH)	*r*(O′H)	*d*(HOCO)	*q*(N)	*q*(H)	*q*(C)
$\mathbf{1}_{exptl}$	84	231	−3	0.266	0.157	0.328
$\mathbf{2}_{exptl}$	84	230	−3	0.267	0.156	0.329
1	97	236	0	0.251	0.199	0.329
2	97	236	0	0.252	0.199	0.329

[a] The *r*(OH) distance is the intramolecular distance of the OH group. The *r*(O′H) distance is the distance from the OH proton to the carboxylate oxygen. The HOCO dihedral angle is also given in degrees. *q*(H) is the charge on the proton of the OH group, and *q*(C) is the charge on the carbon atom of the carboxylate group.

set. Upon hydration the dipole moment is reduced, which is in agreement with their experimental data.

We investigated the ion pairs in [Hbet][Tf_2N] extracted from the crystal structure with a single-point calculation and after optimization. Furthermore, conformers were randomly generated. We selected from the random conformers some examples of ion pairs that show the least similarities with the experimental structures to gain a comparison. In Figure 8, some investigated structures are depicted. The perspective is always chosen such that the S−N−S motif of the anion lies in the same plane, except for structure **5**, which is shown from a different angle, since from the same point of view as shown for the other structures (see inlet) the interaction pattern is not obvious. We observe that in the experimental structures **1** and **2** the betaine cation only interacts with the anion via the carboxylate group. The three methyl groups stay furthest away. This is also evident from the N−N distances listed in Table 4. These structures result

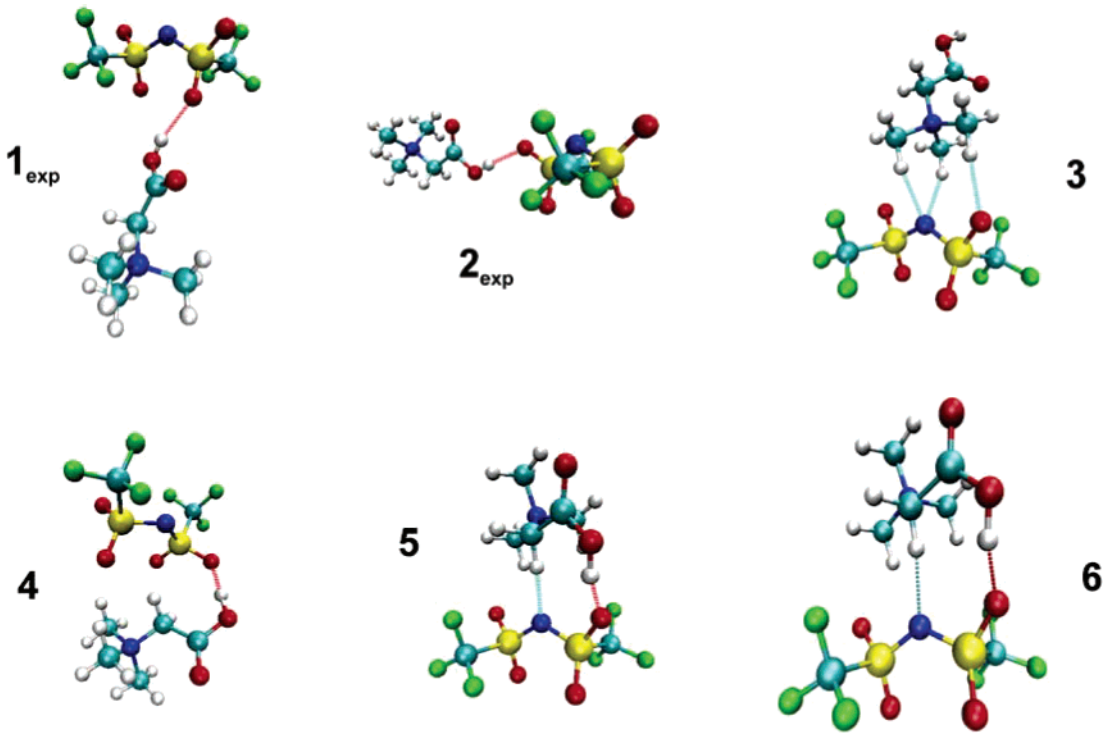

Figure 8. Experimental ion pairs $\mathbf{1}_{exptl}$ and $\mathbf{2}_{exptl}$ and calculated ion pairs **1**−**6** of [Hbet][Tf_2N] (see also Table 4). Ion pairs $\mathbf{2}_{exptl}$ and **2** look very similar; therefore, only one of them has been depicted. All calculated structures were obtained from B3LYP/TZVP calculations.

TABLE 4: Interaction Energies E_I (kJ mol^{-1}) and Parameters of Hydrogen Bonding of Cation−Anion Pairs in [Hbet][Tf_2N][a]

pair	E_I	r(OH)	a(OHO)	σ	r(SO)	a(SNS)	r(NN)	r(CN)
$\mathbf{1}_{exptl}$	−233.8	188	163	0.0237	144	124	812	559
$\mathbf{2}_{exptl}$	−222.0	188	175	0.0308	144	125	831	579
1	−334.9	171	152	0.0823	149	127	457	365
2	−289.8	141	178	0.2413	151	124	814	560
3	−310.1	220	174		148	126	366	609
4	−325.8	189	140	0.0473	149	121	550	445
5	−386.5	171	177	0.0805	149	122	482	442
6	−381.0	167	165	0.0892	149	124	382	428

[a] The distances are given in picometers and angles in degrees. Experimental structures marked with the subscript "exptl" were treated with a single-point calculation; i.e., no optimization was applied. The SEN (σ, e) is also given. All data are from B3LYP/TZVP calculations.

from environmental effects. Since no neighbor is present in the isolated clusters, it is obvious that the ion pair tries to build conformers where as many contacts as possible are formed to gain most of the attractive interaction energy. Ion pair **3** is a special case, because it is the only conformer where the carboxylate group of the betaine is further away from the anion than the nitrogen atom. This conformer is expected to be less stable than the others for the reason that it lacks the strong hydrogen bond of the carboxylate group but also is the most positive atom furthest away, and thus, it will lack Coulombic attraction as compared to the other conformers.

Some geometrical parameters for the investigated ion pairs are presented in Table 4. Ideal hydrogen bond distances r(OH) and angles a(OHO) are observed for ion pairs **5** and **6**. The r(OH) distance of ion pair **3** is measured from a C−H group instead of from the carboxyl group and displays the parameters for a typical weak C−H···O hydrogen bond. If we compare the S−O distance where the hydrogen bond is accepted by the isolated anion, we observe a slight elongation of this bond (for instance, for ion pair **2**). The N−N distances are much shorter for the optimized ion pairs **1** (which largely rearranges) and **3**−**6** than for the experimentally observed structures, which is due to the fact that the ions gain attractive interaction energy if they manage to approach each other to a certain extent in the isolated molecule calculation. As discussed earlier, the r(N−S) distances for the optimized anion structures in the complexes are now even more increased instead of decreased, which can be caused by the inaccurate computational model, but which is most often due to the fact that we have been treating isolated pairs at a temperature of 0 K in our calculations instead of the liquid or the solid phase. The ion pair $\mathbf{1}_{exptl}$ is slightly stronger interacting than the ion pair $\mathbf{2}_{exptl}$. To get an idea of how important the "right" orientation of the betaine toward the anion is, the ion pairs **3** and **6** have to be compared. In both conformers the anion holds the same configuration, such that we almost can qualitatively extract the effect of carboxylate hydrogen bonding as opposed to ammonium hydrogen bonding. The difference in interaction energy is about 70 kJ mol^{-1}, which supports the arguments given before for an arrangement with the carboxylate group close to the anion.

The dipole moments are largest in the ion pair **2** of the optimized conformers (Table 5). Here the ions are more separated from each other than in the other pairs. Comparing again ion pairs **3** and **6**, we find a larger dipole in **3** than in **6**, since the most charged atoms are more separated in ion pair **3** than in ion pair **6**. For $\mathbf{1}_{exptl}$, $\mathbf{2}_{exptl}$, and **2** the absolute value of the charge on the nitrogen atom of the anion is decreased, whereas for ion pairs **1** and **3**−**6** it is increased. The charge on the oxygen atom from the anion that forms a hydrogen bond is almost not changed for the conformers $\mathbf{1}_{exptl}$, $\mathbf{2}_{exptl}$, and **2**.

TABLE 5: Dipole Moments (D) and Charges (au) for the Cation−Anion Pairs in [Hbet][Tf_2N][a]

pair	dipole moment	anion		cation		
		q(N)	*q*(O)	*q*(N)	*q*(H)	*q*(C)
$\mathbf{1}_{exptl}$	31.7	−0.606	−0.506	0.264	0.170	0.308
$\mathbf{2}_{exptl}$	36.0	−0.606	−0.504	0.263	0.169	0.308
1	15.2	−0.684	−0.595	0.257	0.211	0.329
2	30.1	−0.602	−0.478	0.255	0.228	0.315
3	16.7	−0.817	−0.614	0.261	0.111	0.329
4	16.1	−0.618	−0.594	0.343	0.212	−0.032
5	10.7	−0.670	−0.470	0.269	0.187	0.348
6	11.9	−0.703	−0.602	0.313	0.190	0.411

[a] Experimental structures are treated with a single-point calculation.

Contrary to this, conformers **1** and **3**−**6** show strong increased absolute values of the charges on this oxygen atom. For the behavior of the cation we observe in $\mathbf{1}_{exptl}$, $\mathbf{2}_{exptl}$, and **2** that the *q*(N) values are almost unchanged, because the ammonium ion does not directly take part in the ion pair formation. Contrary to this, in ion pairs **4** and **6** the charges are sizably increased. Concerning the behavior of the proton charge, one can say there are large changes in the experimental structure compared to that of the isolated cation, but there is only a negligible difference from that of the isolated cation in the other conformers. Please note that **3** is measured from another proton so that here the comparison to the data from Table 3 is not valid. The charge on the carbon atom of the carboxylate group decreases a little in the experimental conformers, no change is observed for ion pair **3**, and an increase can be observed for ion pairs **5** and **6**. The changes in the carboxylate group in comparing the isolated cation with **5** and **6** can also be due to the fact that the carboxylate groups are oriented in directions different from those of the carboxy groups of **5** and **6**. Structure **4** even contains a negative value on the carbon atom. The shared electron number that can be used as an indicator for hydrogen bonding at reasonable distances confirms our observed trends. In our set of conformers, also ion pairs that hold the anions in a cisoid conformation are presented (for example, ion pair **4**)**.** Although this *cis*-form is more strongly bound, the shared electron number σ given in Table 4 has a smaller value than those for the other optimized pairs. A smaller shared electron number indicates a weaker hydrogen bonding.[86]

Thermomorphic Behavior. Although we described in one of the previous sections that [Hbet][Tf_2N] forms a two-phase system with water, this statement is only true for mixtures at room temperature and slightly above. Upon heating the mixture, a one-phase-system with an upper consolute point at 55.5 ± 0.2 °C is formed. Cooling of the one-phase mixture resulted again in phase separation. The phase separation is illustrated in Figure 9. The phase diagram of the binary system [Hbet]-[Tf_2N]−water is shown in Figure 10. The phase diagram was measured by equilibrating the [Hbet][Tf_2N]−water mixture at a given temperature, followed by analysis of the components in the [Hbet][Tf_2N]-rich phase (lower layer) and in the water-rich phase (upper layer). The composition of the phases was determined by distilling out the water and comparing the original mass with the remaining (nonvolatile) ionic liquid mass. At the critical concentration, the mass fraction of the ionic liquid is 0.519 ± 0.001.

Apart from their feasibility for phase separation in view of applications, also the fundamental physical chemistry behind phase separation is interesting. Phase separation of binary liquid mixtures has been an important research issue for several decades,[87,88] in particular the theoretical and experimental

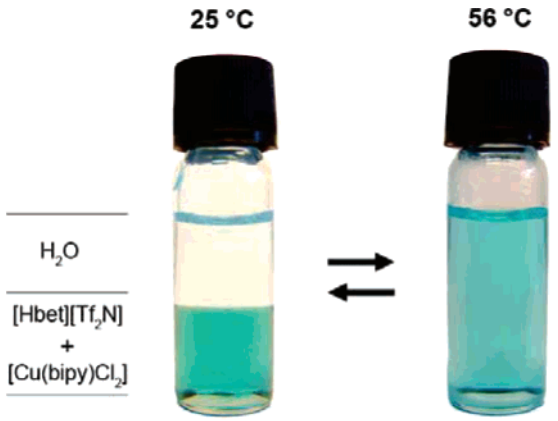

Figure 9. Temperature-dependent phase behavior of a binary [Hbet]-[Tf_2N]−water mixture. The blue [Cu(bipy)Cl_2] complex was dissolved in the ionic liquid to accentuate the phase boundaries.

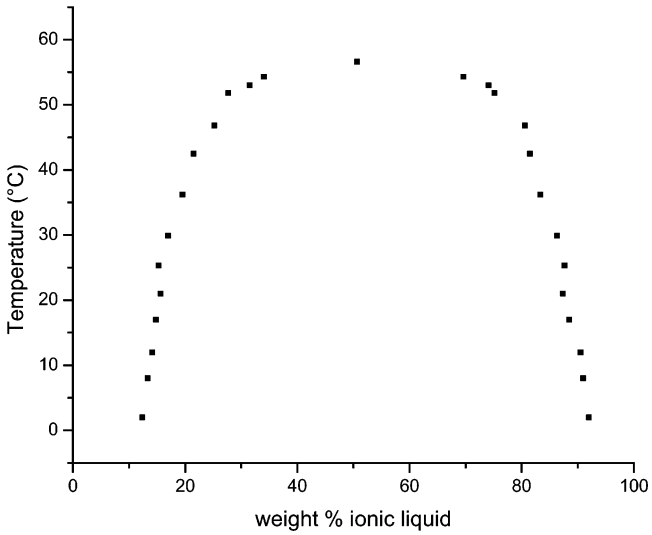

Figure 10. Liquid−liquid equilibrium phase diagram of the binary mixture [Hbet][Tf_2N]−water.

research of the phase transition behavior. In general, it is expected that the critical behavior of the physical properties of binary liquid mixtures around the critical point can be described by a power law, with universal exponents that can be classified as Ising-like. For the specific heat capacity *c* there are many experimental confirmations for the theoretically predicted Ising exponent $\alpha = 0.110$.[88,89] The expected power law with Ising-like critical exponent β for the order parameter, i.e., the concentration difference of one of the two compounds between the coexisting phases, has been mainly verified via the dielectric permittivity and has also been confirmed.[90] There have also been suggestions for the existence of a critical anomaly in the thermal conductivity κ in the mixed phase.[91,92] However, recent high-resolution precision experiments on several binary liquid mixtures have shown the absence of this anomaly.[73,74] Moreover, these experiments have shown that, in the phase-separated temperature region, the thermal conductivity difference between the two phases follows a power law with critical exponent β. This confirms expectations that also the thermal conductivity difference between the coexisting phases is an appropriate measure for the order parameter and the concentration. This observation is quite promising for in situ concentration-monitoring purposes.

The investigation of the temperature dependence of the thermal effusivity and thermal conductivity of the binary liquid mixture [Hbet][Tf_2N]−water was aimed to resolve three issues.

First, the relationship between the concentration and the thermal conductivity was determined, by comparing these two quantities for the mixture at different temperatures. Second, it was verified whether both these quantities can be used to determine the exponent β in the expected power law, like in the binary liquid mixtures consisting of nonionic liquids. Third, also the critical behavior (or its absence) of the thermal conductivity and effusivity in the mixed phase was verified.

The thermal conductivity, thermal effusivity, and specific heat capacity at constant pressure of the binary mixture [Hbet][Tf_2N]−water was studied by the *front-detection photopyroelectric* (FPPE) technique. In this technique, the electrical current response $I(t)$ of the pyroelectric detector to the absorbed electromagnetic radiation (light), modulated at a frequency ω, can be written as

$$I(t) = \frac{pI_0S_p}{2L_p\rho_p c_p}\Gamma(\omega)\, e^{i\omega t} \quad (1)$$

Here, ρ_p and c_p are the density and the specific heat capacity of the sensor, respectively, I_0 is the radiation intensity amplitude, p is the pyroelectric coefficient, and S_p and L_p are the (illuminated) sensor area and its thickness. The configuration is considered as a one-dimensional one because the thermal diffusion lengths of the sensor and the other layers are small compared to their lateral dimensions. The thin liquid sample is sandwiched between the sensor (on both sides coated by chromium) and a thermally thick layer (several millimeters) of a material with high heat capacity and thermal conductivity, which serves as a heat sink. On the other side of the sensor, there is a thermally thick air layer. The chromium electrode at the interface between the air layer and the sensor absorbs modulated infrared radiation and thus serves as a modulated heat source. In eq 1, $\Gamma(\omega)$ is a dimensionless factor proportional to the frequency-dependent average temperature in the pyroelectric sensor and is a function of the different layers in the configuration.[73] At appropriately chosen modulation frequencies, one obtains the thermal effusity of the sample e_s:

$$e_s = (\kappa_s\rho_s c_s)^{1/2} \quad (2)$$

Here, κ_s is the thermal conductivity of the sample, ρ_s is the density of the sample, and c_s is the heat capacity of the sample.

Two measuring modes can be considered: the thermal conductivity mode and the thermal effusivity mode. In the *thermal conductivity mode*, the modulation frequency is low (0.36 Hz). The pyroelectric signal is in this case only sensitive to the thermal resistance L_s/κ_s of the sample and is independent of its heat capacity. L_s is the sample thickness, and κ_s is its thermal conductivity. In the *effusivity mode*, the modulating frequency is higher (3 Hz) and the backing (heat sink) plays no role in the pyroelectric signal. In this case, the sample properties only appear through the ratio $b_{sp} = e_s/e_p$, where e_s is the effusity of the sample and e_p is the effusity of the pyroelectric sensor. For applying the pyroelectric technique, the thermal properties of the detector, heat sink, and air, as well as L_p and L_s, have to be known. Proper values can be obtained from the literature and/or from calibration runs (without sample or with reference samples).

Figure 11 shows that the measured thermal conductivity varies quite linearly with the determined concentration, confirming that the thermal conductivity is a suitable property for monitoring the concentration and order parameter. From the data in Figure 12 we also fitted a power law to the thermal conductivity difference between the two phases and found the results

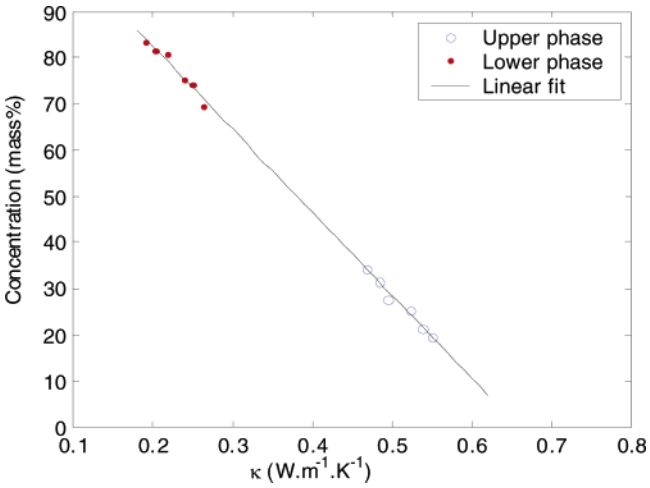

Figure 11. Correlation plot between concentration and thermal conductivity.

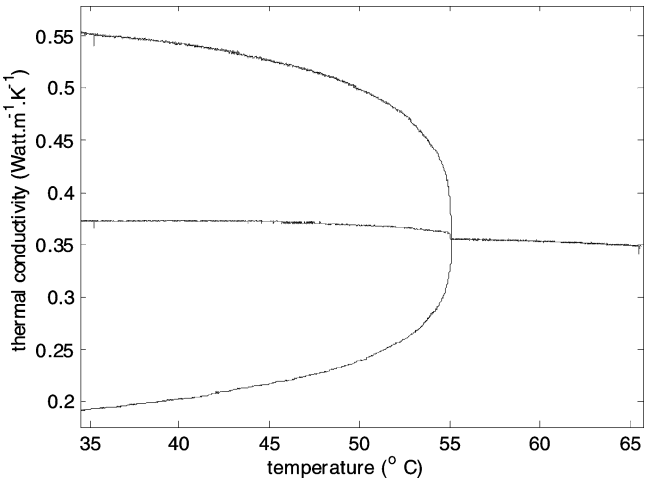

Figure 12. Temperature dependence of the thermal conductivity of the [Hbet][Tf_2N]−water mixture. With decreasing temperature, below the phase transition, increasingly water-rich and [Hbet][Tf_2N]-rich phases separate. The middle curve is the average of the two curves in the phase-separated region. Note that the average thermal conductivity does not show a peak around the critical temperature.

consistent with the theoretically predicted 3-dimensional Ising model exponent $\beta = 0.325$. Further details on the analysis of these data will be given in a forthcoming paper. Our result for the critical exponent β confirms earlier observations on other ionic liquid phase-separating binary mixtures.[93,94] For this mixture, the ionic character of one of its compounds does not seem to modify the critical behavior. Apparently the separation of the anions and cations by the surrounding water molecules does not influence the correlation length of the water−IL concentration fluctuations. This suggests that the cations and anions act as paired entities (ion pairs). Future research could reveal the influence of a significant presence of protons or hydroxide ions, by changing the pH of the mixture. Also the temperature dependence of the thermal effusivity reveals the phase transition.

The thermal effusivities of the two sample regions in Figure 13 reveal both the phase separation below the consolute point and the anomaly in the specific heat capacity around the consolute point. A detailed analysis of the critical behavior of the specific heat capacity, determined from our thermal effusivity and conductivity data, supported by adiabatic calorimetry (ASC) results, will be published elsewhere.

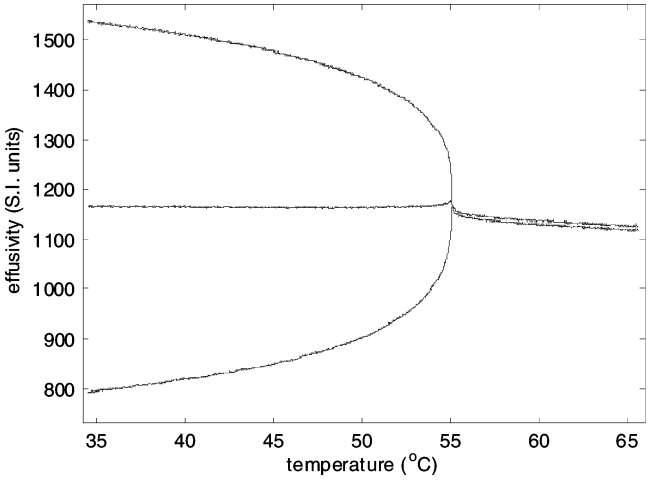

Figure 13. Temperature dependence of the thermal effusivity of the [Hbet][Tf_2N]−water mixture. With decreasing temperature, below the phase transition, increasingly water-rich and [Hbet][Tf_2N]-rich phases separate. The middle curve is the average of the two curves in the phase-separated region. Note the small peak around the phase transition temperature, due to the critical behavior of the specific heat capacity.

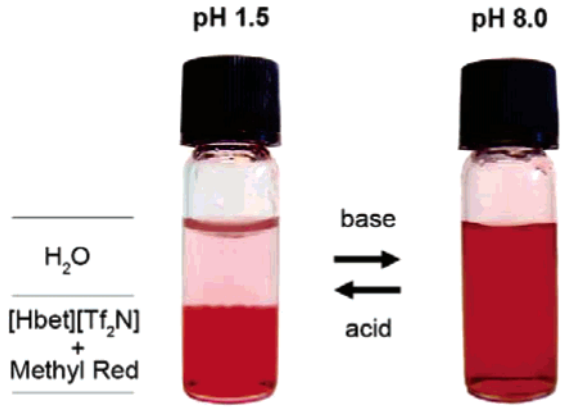

Figure 14. Illustration of the pH-dependent phase behavior of a binary [Hbet][Tf_2N]−water mixture. A two-phase system is obtained for acidic and neutral conditions, whereas a one-phase system is observed for alkaline conditions (pH > 8). The dye methyl red was added to make the phase boundaries more visible.

pH-Dependent Phase Behavior. When a biphasic mixture of protonated betaine bis(trifluoromethylsulfonyl)imide is treated with a solution of the alkali-metal hydroxide LiOH, NaOH, or KOH, a monophasic mixture is obtained, because the alkali-metal salts of betaine bis(trifluoromethylsulfonyl)imide are water soluble (Figure 14). Acidification of the solution leads to the regeneration of the hydrophobic protonated betaine bis(trifluoromethylsulfonyl)imide ionic liquid and thus to phase separation. This pH-dependent phase behavior of the ionic liquid is not unexpected. Treatment of a solution of a carboxylic acid in diethyl ether with an aqueous solution of sodium hydroxide or sodium hydrogen carbonate also transfers the carboxylate from the organic phase to the aqueous phase.

Solubility of Metal Oxides. An interesting property of betaine bis(trifluoromethylsulfonyl)imide is its ability to dissolve metal oxides. The metal oxides react with the carboxylic acid group of the ionic liquid to form carboxylate complexes and water. The following oxides were found to be soluble in the ionic liquid [Hbet][Tf_2N]: Sc_2O_3, Y_2O_3, La_2O_3, Pr_6O_{11}, Nd_2O_3, Sm_2O_3, Eu_2O_3, Gd_2O_3, Tb_4O_7, Dy_2O_3, Ho_2O_3, Er_2O_3, Tm_2O_3, Yb_2O_3, Lu_2O_3, UO_3, PbO, ZnO, CdO, HgO, CuO, Ag_2O, NiO, PdO, and MnO. In a typical experiment, the metal oxide is mixed with [Hbet][Tf_2N] and water, and the mixture is stirred for several hours. After evaporation of water under reduced pressure, a solution of the metal betaine complex in [Hbet][Tf_2N] is obtained. The solubility of metal oxides in protonated betaine bis(trifluoromethylsulfonyl)imide is high because the ionic liquid can form stoichiometric compounds with the metals; i.e., a large amount of metal oxide can be added to the [Hbet][Tf_2N] ionic liquid until all the ionic liquid is transformed into a metal complex. However, the presence of water facilitates the dissolution of the metal oxide in the ionic liquid. It is much more difficult to dissolve the ionic liquid in direct contact with the metal oxide. This can be due to the fact that most metal oxides have a hydrophilic surface, whereas the ionic liquid is hydrophobic; therefore, the wettability of the metal oxide by the pure ionic liquid is poor. Direct dissolution (i.e., without addition of water) of a metal oxide in [Hbet][Tf_2N] was observed for CuO. Not all metal oxides can be solubilized in [Hbet][Tf_2N]. Insoluble or very poorly soluble are iron and cobalt oxides, as well as aluminum oxide and silicon oxide. Besides the metal oxides, also different metal salts such as $CuCl_2 \cdot 2H_2O$ or $EuCl_3 \cdot 6H_2O$ are soluble in [Hbet][Tf_2N], although the solubility of the metal salts is appreciably lower than that of the metal oxides. For instance, [Hbet][Tf_2N] can dissolve 1.75 mol % $CuCl_2$ and 6 mol % $EuCl_3$ (determined titrimetrically by EDTA).

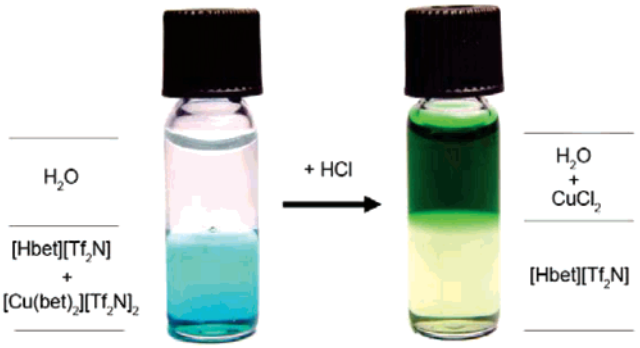

Figure 15. Transfer of copper(II) from the ionic liquid [Hbet][Tf_2N] to the aqueous phase upon acidification of the aqueous phase by a hydrogen chloride solution.

The metals can be stripped from betaine bis(trifluoromethylsulfonyl)imide by extracting the ionic liquid with an acidified aqueous solution (for instance, with diluted hydrochloric acid or diluted nitric acid). The metal complex of protonated betaine bis(trifluoromethylsulfonyl)imide is decomposed, and the betaine bis(trifluoromethylsulfonyl)imide ionic liquid is regenerated. The metal ion is thus transferred to the aqueous phase. For instance, a solution of copper(II) in [Hbet][Tf_2N] was extracted twice with a 37% HCl solution. The ratio of the metal content in the aqueous phase to the ionic liquid phase was determined by titration to be 1:82 after the first extraction. The metal was almost completely extracted to the aqueous phase after a second extraction with the acidic solution. The transfer of copper(II) from the ionic liquid to the aqueous phase upon acidification of the aqueous layer is shown in Figure 15. The same extraction can also be done with aqueous HNO_3 or H_2SO_4. A nearly quantitative removal of neodymium(III) from [Hbet][Tf_2N] could be obtained by two extractions of the ionic liquid with a 37% HCl solution. The [Hbet][Tf_2N] ionic liquid can be reused after stripping of its metal content. The ability of protonated betaine bis(trifluoromethylsulfonyl)imide to dissolve metal oxides can be used to clean oxidized metal surfaces. For instance, a copper sheet covered with a black coating of copper(II) oxide could be cleaned after short immersion in protonated betaine bis(trifluoromethylsulfonyl)imide.

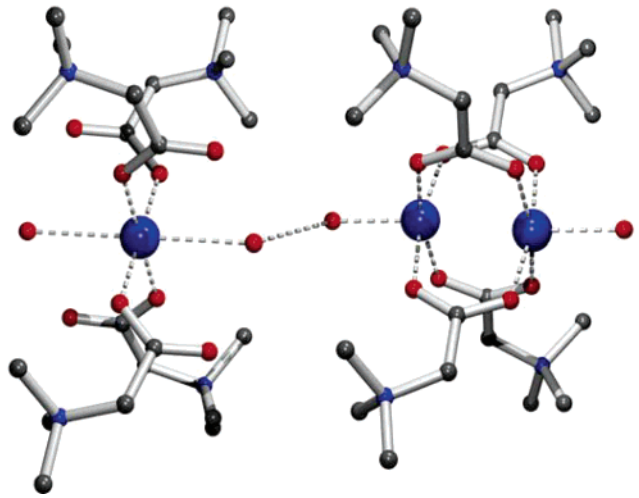

Figure 16. Hydrogen bonding between alternating $[Cu(bet)_4(H_2O)_2]^{2+}$ and $[Cu_2(bet)_4(H_2O)_2]^{4+}$ cations along the *c*-axis in the crystal structure of $[Cu(bet)_4(H_2O)_2][Cu_2(bet)_4(H_2O)_2][Tf_2N]_6$.

Characterization of Metal Complexes. Complexes of [Hbet][Tf_2N] were prepared for different metals. The general synthetic procedure consisted of stirring stoichiometric amounts of the metal oxide and [Hbet][Tf_2N] in water at reflux temperature for 12 h. The metal salts were obtained after evaporation of water. The metal complexes of betaine bis(trifluoromethylsulfonyl)imide have in general a high melting point (>100 °C), but the rare-earth complexes of betaine bis(trifluoromethylsulfonyl)imide have melting points below 100 °C and can thus be considered as genuine ionic liquids. An overview of the melting points is given in the Supporting Information.

Although it was not the purpose of this study to investigate the crystal chemistry of metal complexes of protonated betaine bis(trifluoromethylsulfonyl)imide, we determined the crystal structures of the copper(II) and dysprosium(III) complexes to illustrate that d-block or f-block elements form well-defined complexes by interaction with the [Hbet][Tf_2N] ionic liquid.

Single crystals of the compound $[Cu(bet)_4(H_2O)_2][Cu_2(bet)_4(H_2O)_2][Tf_2N]_6$ suitable for X-ray diffraction were obtained from an aqueous solution of the copper(II) betaine complex after it was left to evaporate at room temperature. The crystal structure of $[Cu(bet)_4(H_2O)_2][Cu_2(bet)_4(H_2O)_2][Tf_2N]_6$ consists of $[Cu(bet)_4(H_2O)_2]^{2+}$ and $[Cu_2(bet)_4(H_2O)_2]^{4+}$ cations and bis(trifluoromethylsulfonyl)imide anions. In the monomeric cation $[Cu(bet)_4(H_2O)_2]^{2+}$, the copper(II) ion is coordinated by four carboxylate oxygen atoms at the basal plane (average d(Cu(2)−O) = 1.95 Å) and has two weak contacts to aqua ligands at the apical position (average d(Cu(2)−O = 2.66 Å) to give a distorted octahedral 4 + 2 coordination. In the dimeric $[Cu_2(bet)_4(H_2O)_2]^{4+}$ cations, the copper(II) ions are quadruply bridged by μ_2-carboxylate groups of the bet zwitterions (d(Cu−Cu) = 2.66 Å). The coordination sphere of the copper ions is completed by one additional water molecule coordinating to each copper(II) ion (d(Cu−O) = 2.13 Å). This dimeric subunit is somewhat similar to the well-known $[Cu_2(\mu_2\text{-carboxylate})_4]$ complexes,[95,96] with one additional water molecule coordinating to each copper(II) ion. The cations $[Cu(bet)_4(H_2O)_2]^{2+}$ and $[Cu_2(bet)_4(H_2O)_2]^{4+}$ are alternately connected by hydrogen bonding between the coordinating water molecules (d(O−O) = 2.66 Å) and form polymers along the *c*-axis. The bis(trifluoromethylsulfonyl)imide anions surround these rows without showing any hydrogen bonding. The molecular structure of the cations in $[Cu(bet)_4(H_2O)_2][Cu_2(bet)_4(H_2O)_2][Tf_2N]_6$ is shown in Figure 16. The X-ray powder pattern of the bulk product that was obtained by mixing stoichiometric amounts of copper(II) oxide and [Hbet][Tf_2N] in water at refluxing temperature was measured. Indexing of the powder diffractogram gave for the solid compound a unit cell with the following parameters: a = 15.23(7) Å, b = 26.13 (7) Å, c = 15.57(6) Å, β = 117.76(2)°. These values compare reasonably well with those of the $[Cu(bet)_4(H_2O)_2][Cu_2(bet)_4(H_2O)_2][Tf_2N]_6$ single crystal: a = 15.2183(2) Å, b = 26.1383(3) Å, c = 15.6211(2) Å, β = 117.5540(10)°. These data indicate that the compound obtained by crystallization from an aqueous solution has the same composition as the one obtained from the bulk ionic liquid.

The compound $[Dy_2(bet)_8(H_2O)_4][Tf_2N]_6$ crystallized from an aqueous solution of the dysprosium(III) betaine complex after it was left to evaporate at room temperature. The structure consists of dimeric $[Dy_2(bet)_8(H_2O)_4]^{6+}$ cations and bis(trifluoromethylsulfonyl)imide anions. In the crystal structure, each dysprosium(III) ion is surrounded by six monodentate coordinating betaine zwitterions; four of them are μ_2-bridging so that dysprosium(III) ions occur as dimers. Additionally, two water molecules are coordinated to each of the dysprosium(III) ions. One of these water molecules on each side of the dimer forms weak hydrogen bonds to the oxygen of one of the bis(trifluoromethylsulfonyl)imide anions (d(O···O) = 2.87 Å). The coordination number of dysprosium(III) is eight and the coordination polyhedron of the dysprosium(III) ion can be described as a slightly distorted square antiprism. The cationic dimer $[Dy_2(bet)_8(H_2O)_4]^{6+}$ in the crystal structure of $[Dy_2(bet)_8(H_2O)_4][Tf_2N]_6$ is shown in Figure 17. The X-ray powder pattern of the bulk product that was obtained by mixing stoichiometric amounts of dysprosium(III) oxide and [Hbet][Tf_2N] in water at refluxing temperature indicates that the bulk product consists of two different phases, one being the $[Dy_2(bet)_8(H_2O)_4][Tf_2N]_6$ phase and one an unidentified phase.

Discussion

[Hbet][Tf_2N] is accessible via different synthetic routes. The best method is by reaction of the zwitterionic betaine with the acid hydrogen bis(trifluoromethylsulfonyl)imide, Tf_2NH. This reaction involves a simple proton transfer from the bis(trifluoromethylsulfonyl)imide to the more basic carboxylate group, so that the betaine will be protonated. This method is generally applicable for the preparation of other betaine salts. For instance, we prepared by this method protonated betaine hexafluorophosphate, protonated betaine triflate, and protonated betaine pentafluorobenzoate. However, we did not consider all these salts further in detail, because they all have melting points above 100 °C. A second synthetic route to the protonated betaine bis(trifluoromethylsulfonyl)imide ionic liquid is by the metathesis reaction of betaine hydrochloride and lithium bis(trifluoromethylsulfonyl)imide (in 1:1 molar ratio) in aqueous solution. The ionic liquid separates from the aqueous layer due to its hydrophobicity. The ionic liquid prepared by the metathesis reaction has a melting point of 57 °C, and the compound can easily be supercooled to room temperature. The fact that $[(Hbet)_3(bet)][Tf_2N]_3$ is formed besides [Hbet][Tf_2N], depending on the experimental conditions, leads to the assumption that an equilibrium between different species in solution is present. So far, no detailed information on this equilibrium is available yet. The pure $[(Hbet)_3(bet)][Tf_2N]_3$ compound (mp 70 °C) crystallizes from a solution of the mixture in the [C_4mim][Tf_2N] ionic liquid. Pure [Hbet][Tf_2N], free of $[(Hbet)_3(bet)][Tf_2N]_3$, can be obtained by mixing stoichiometric amounts of the betaine inner salt (bet) and Tf_2NH. Pure [Hbet][Tf_2N] melts at 69 °C.

The crystal structure of $[(Hbet)_3(bet)][Tf_2N]_3$ has been described in the Results. The compound $[(Hbet)_3(bet)][Tf_2N]_3$

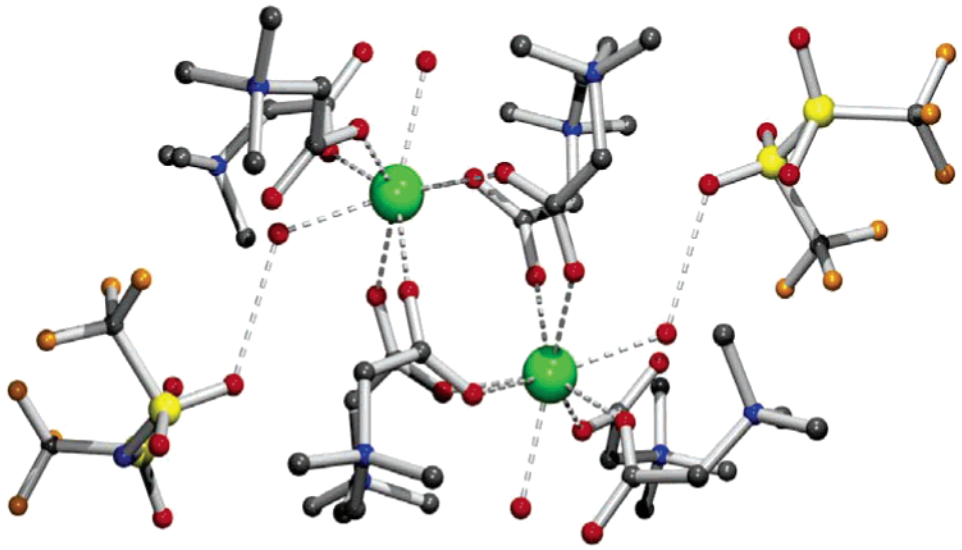

Figure 17. Cationic dimer $[Dy_2(bet)_8(H_2O)_4]^{6+}$ in the structure of $[Dy_2(bet)_8(H_2O)_4][Tf_2N]_6$ with hydrogen bonding from coordinated water molecules to two bis(trifluoromethylsulfonyl)imide anions.

can be considered as consisting of 3 equiv of [Hbet][Tf_2N] and 1 equiv of the betaine zwitterion. Interestingly, this additional betaine zwitterion alters the type of hydrogen bonding from exclusive anion−cation interactions in [Hbet][Tf_2N] to solely $[(Hbet)_3(bet)]^{3+}$ cationic interactions with betaine tetramers sharing three protons. Hydrogen bonding is an important structural feature in the solid-state structures of the betaine bis(trifluoromethylsulfonyl)imide complexes. Strong hydrogen bonding was also observed in other crystal structures of betaine compounds, such as betaine hydrochloride,[97] betaine trifluoroacetate,[98] and betaine perchlorate monohydrate.[99] Although the dimeric Hbet−bet structure has been reported for [(Hbet)(bet)]-[C_2O_4H] (where C_2O_4H is hydrogen oxalate)[100] and different types of hydrogen bonding for betaine have been discussed in the literature,[101] to the best of our knowledge no tetrameric unit has been reported yet.

Quantum chemical calculations show that the bis(trifluoromethylsulfonyl)imide anion is most suitable for a coordination if the CF_3 groups are arranged in a *trans*-fashion (see Figure 6, electron density mapped with electrostatic potential for anion conformers **1** and **4**). These structures are also energetically favorable. An excellent overview of quantum chemical calculations on $[Tf_2N]^-$ complexes is provided by Fujii et al.[102] Several authors found a cisoid and a transoid conformation for $[Tf_2N]^-$ or related anions.[102−106] These authors conclude from their calculations that the transoid conformation (as, for example, in our conformer **1**) is a few kJ mol^{-1} more stable than the cisoid conformation (as, for example, in our conformer **4**). This is in agreement with our calculations. Geometrical parameters of our optimizations are in the same range as those obtained by others.[102,103,105] The charges and ELF[80−82] indicate that the most negative atom of the bis(trifluoromethylsulfonyl)imide group is the nitrogen atom. The oxygen atoms are preferred over the fluorine atoms as the interaction site, because there is more negative charge, and they have higher localized electron pairs. The oxygen atom is sterically more favored than the nitrogen atom for interaction with the cation (see the ELF pictures in Figure 5). It is obvious from them that the doughnut-shaped rings that represent the lone pairs can be approached from all sides, whereas the nitrogen lone pairs can be reached from one side only. The protonated betaine cation will try to interact with the carboxylate group, since the carbon atom from the carboxylate group has the highest positive charge. From the electrostatic potential, hydrogen bonding by the carboxylate group is obvious, since the carboxylate proton is very positively polarized. Interaction of the anion with the cation at the side of the ammonium group is possible. This can be observed from the dark (blue) areas in Figure 7. This is the reason in the gas phase where no concurrent neighbor is present the protonated betaine cation also interacts with the ammonium group. However, the carboxylate proton is predestinated for hydrogen bonding, since the blue area forms a bulge, whereas the ammonium displays blue areas only at a dent of the electron density. Judging from the calculated interaction energy, coordination with the carboxylate group is favorable by 70 kJ mol^{-1}. If the interaction takes place as in the experimental structure, the charges are reduced. This reduction might be due to charge transfer. This theoretical study of the betaine−bis(trifluoromethylsulfonyl)-imide ion pair complements earlier quantumchemical studies on ion pairing in ionic liquids.[107−112] Holbrey and co-workers found examples of ionic liquids that adopt the cisoid conformation of the $[Tf_2N]^-$ anion.[113] The cation arranges toward the anion such that a bifurcated hydrogen bond can be formed. The authors conclude that their results provide evidence for the flexibility of the anion in the crystal state. Deetlefs et al. investigated with the aid of neutron diffraction the structure of the ionic liquid formed by the $[Tf_2N]^-$ anion and the 1,3-dimethylimidazolium cation.[114] For their interpretation they used two different sets of charges, one that agrees very well with our trends (set B) and one that seems to be more counterintuitive (set A). Fixed charges are problematic for the description of liquids, since the charges change very much due to polarization.[115,116] The authors found that the anion prefers to be in the *trans* conformation. They state that it is not possible to draw easily conclusions for the liquid state from the solid state. And this is certainly also valid for isolated molecule calculations.

The thermomorphic behavior and the pH switching of the ionic liquid [Hbet][Tf_2N] in its mixtures with water are strongly related to hydrogen bonding.[117] Köddermann et al. investigated different ionic liquids mixed with water and showed that hydrogen bonding can play an important role in ionic liquids.[118] In [C_2mim][Tf_2N] different types of structures were found. There exists a double-donor conformer in which the water molecules form two hydrogen bonds to one $[Tf_2N]^-$ group. In another conformer, i.e., a single-donor conformer, the water forms one strong hydrogen bond to the anion. Water is also able to function

as an acceptor and a donor between the cation and anion. These findings confirm our results that water under certain conditions is miscible (basic pH) with [Hbet][Tf_2N] and under certain conditions not (low pH). Proton transfer from protonated betaine to molecules with comparable gas-phase basicity was investigated by Price et al.[119] Molecules that are more basic than betaine attract the proton of Hbet and form a so-called salt bridge or an ion−zwitterion interaction (baseH^+···bet), whereas molecules that are less basic form a Hbet−base complex, i.e., an ion−molecule complex. The ion−molecule complexes usually prefer to interact with the quaternary nitrogen of betaine. The temperature-dependent phase behavior of [Hbet][Tf_2N]−water mixtures could be exploited for chemical separations. The thermophysical investigations presented in this paper show that this system with an upper consolute point behaves similarly to binary mixtures with an upper consolute point which consist of water and a (nonionic) molecular liquid. There is currently a strong interest in phase switching of ionic liquids and organic solvents (or water), because of its importance for product separation. The most detailed studies on the temperature-dependent miscibility of ionic liquids with organic solvents have focused on alcohols as solvents.[120] Brennecke and co-workers illustrated that carbon dioxide can induce the formation of an ionic-liquid-rich phase and an organic-rich liquid phase in mixtures of methanol and 1-butyl-3-methylimidazolium hexafluorophosphate.[121,122] A similar behavior was observed when methanol was replaced by water.[123] Because gaseous carbon dioxide can cause a phase separation in organic and aqueous solutions containing ionic liquids at relatively low pressures (<5.2 MPa), it can be expected that carbon dioxide can further improve the phase separation of the [Hbet][Tf_2N]−water binary mixtures. The phase behavior that we observe for the [Hbet][Tf_2N]−water binary mixtures is very reminescent of the behavior observed by Suarez et al. for [C_4mim][BF_4]−water binary mixtures.[124] In that case, an upper consolute point of 5 °C was reported.

An interesting property of the protonated betaine bis(trifluoromethylsulfonyl)imide ionic liquid is its ability to dissolve metal oxides. However, the metal-solubilizing power is selective: not all metal oxides are soluble in the ionic liquid. Soluble are oxides of the trivalent rare earths, uranium(VI) oxide, zinc(II) oxide, cadmium(II) oxide, mercury(II) oxide, nickel(II) oxide, copper(II) oxide, palladium(II) oxide, lead(II) oxide, manganese(II) oxide, and silver(I) oxide. Insoluble or very poorly soluble are iron(III), manganese(IV), and cobalt oxides, as well as aluminum oxide and silicon oxide. Also metal hydroxides can be solubilized in the ionic liquid.

Given the interest in ionic liquids prepared from cheap, easily accessible, and preferentially renewable starting products, one may wonder why betaine ionic liquids have not been considered before, in contrast to the choline ionic liquids. This can probably be explained by the high melting points of most betaine salts. Only by the unique combination of a protonated betaine cation and a bis(trifluoromethylsulfonyl)imide anion can a low-melting-point ionic liquid be obtained. We mentioned above that combinations of betaine with other fluorinated cations such as hexafluorophosphate give salts with melting points well above 100 °C.

Metal complexes with the zwitterionic ligand betaine have attracted researchers for a long time,[125−130] but none of these complexes contain the bis(trifluoromethylsulfonyl)imide anion. We present in this paper the crystal structures of a copper(II) and a dysprosium(III) complex of betaine to illustrate the variety of structures that can be formed with the zwitterionic betaine ligand. We are presently further exploring the rich coordination chemistry of the metal complexes formed by reaction between a metal oxide and [Hbet][Tf_2N]. It should be noticed that also heteronuclear copper−lanthanide complexes of betaine are known.[131]

Conclusions

[Hbet][Tf_2N] is a versatile task-specific ionic liquid that can be used for the selective solubilization of metal oxides and metal salts. The concept of solubilizing metal oxides in a task-specific ionic liquid is based on the presence of acidic functional groups in the ionic liquid. Moreover, the ionic liquid can be switched from a hydrophobic one to a hydrophilic one by temperature or pH control. Although the melting point of [Hbet][Tf_2N] is above room temperature, it is miscible with room-temperature ionic liquids containing the $[Tf_2N]^-$ anion, and the mixtures are room-temperature ionic liquids as well. This widely broadens the applicability of this ionic liquid. Further research is being directed to solving the crystal structures of the metal complexes formed by [Hbet][Tf_2N], to speciation of the metal complexes in the ionic liquid, to an in-depth study of the thermophysical properties of [Hbet][Tf_2N]−solvent binary mixtures, to other theoretical methods that allow the description of the liquid phase, and to quantum chemical calculations applied to pairs that display different intermolecular forces.

Acknowledgment. This project was supported by FWO-Flanders (Projects G.0117.03 and G.0125.03) and the Katholieke Universiteit Leuven (Projects GOA 03/03, GOA 2002/04, and IDO/05/005). We gratefully acknowledge the financial support of the DFG priority program SPP 1191 "Ionic Liquids" and the ERA Chemistry program, which allows fruitful collaboration under the project "A Modular Approach to Multi-responsive Surfactant/Peptide (SP) and Surfactant/Peptide/Nanoparticle (SPN) Hybrid Materials". B.K. furthermore acknowledges the financial support under the collaborative research center SFB 624 "Templates" at the University of Bonn.

Supporting Information Available: CIF files and additional figures of the crystal structures, experimental procedures and characterization of metal complexes, melting points of metal-containing ionic liquids (Table S1), and picture of the experimental setup for pyroelectric measurements. This material is available free of charge via the Internet at http://pubs.acs.org.

References and Notes

(1) Seddon, K. R. *J. Chem. Technol. Biotechnol.* **1997**, *68*, 351−356.
(2) Earle, M. J.; Seddon, K. R. *Pure Appl. Chem.* **2000**, *72*, 1391−1398.
(3) Seddon, K. R. *Nat. Mater.* **2003**, *2*, 363−365.
(4) Welton, T. *Chem. Rev.* **1999**, *99*, 2071−2083.
(5) Wasserscheid, P.; Keim, W. *Angew. Chem., Int. Ed.* **2000**, *39*, 3773−3789.
(6) Huddleston, J. G.; Visser, A. E.; Reichert, W. M.; Willauer, H. D.; Broker, G. A. Rogers, R. D. *Green Chem.* **2001**, *3*, 156−164.
(7) Huddleston, J. G.; Willauer, H. D.; Swatloski, R. P.; Visser, A. E.; Rogers, R. D. *Chem. Commun.* **1998**, 1765−1766.
(8) Blanchard, L. A.; Hancu, D.; Beckman, E. J.; Brennecke, J. F. *Nature* **1999**, *399*, 28−29.
(9) Davis, J. H. Jr., Fox, P. A. *Chem. Commun.* **2003**, 1209−1212.
(10) Binnemans, K. *Chem. Rev.* **2005**, *105*, 4148−4204.
(11) Lin, I. J. B.; Vasam, C. S. *J. Organomet. Chem.* **2005**, *690*, 3498−3512.
(12) Forsyth, S. A.; Pringle, J. M.; MacFarlane, D. R. *Aust. J. Chem.* **2004**, *57*, 113−119.
(13) Earle, M. J.; Esperanca, J. M. S. S.; Gilea, M. A.; Lopes, J. N. C.; Rebelo, L. P. N.; Magee, J. W.; Seddon, K. R.; Widegren, J. A. *Nature* **2006**, *439*, 831−834.
(14) Wasserscheid, P. *Nature* **2006**, *439*, 797−797.

(15) Dupont, J.; de Souza, R. F.; Suarez, P. A. Z. *Chem. Rev.* **2002**, *102*, 3667−3691.
(16) Gordon, C. M. *Appl. Catal., A* **2001**, *222*, 101−117.
(17) Carmichael, A. J.; Earle, M. J.; Holbrey, J. D.; Mccormac, P. B.; Seddon, K. R. *Org. Lett.* **1999**, *1*, 997−1000.
(18) Sheldon, R. *Chem. Commun.* **2001**, 2399−2407.
(19) Wasserscheid, P.; Welton, T. *Ionic Liquids in Synthesis*; Wiley-VCH: Weinheim, Germany, 2002.
(20) Olivier-Bourbigou, H.; Magna, L. *J. Mol. Catal. A* **2002**, *182*−*183*, 419−437.
(21) Antonietti, M.; Kuang, D. B.; Smarsly, B.; Zhou, Y. *Angew. Chem., Int. Ed.* **2004**, *43*, 4988−4992.
(22) Taubert, A. *Angew. Chem., Int. Ed.* **2004**, *43*, 5380−5382.
(23) Mudring, A. V.; Babai, A.; Arenz, S.; Giernoth, R. *Angew. Chem., Int. Ed.* **2005**, *44*, 5485−5488.
(24) Cooper, E. R.; Andrews, C. D.; Wheatley, P. S.; Webb, P. B.; Wormald, P.; Morris, R. E. *Nature* **2004**, *430*, 1012−1016.
(25) Endres, F. *Z. Phys. Chem.* **2004**, *218*, 255−283.
(26) Bansal, D.; Cassel, F.; Croce, F.; Hendrickson, M.; Plichta, E.; Salomon, M. *J. Phys. Chem. B.* **2005**, *109*, 4492−4496.
(27) Lee, S.-Y.; Yong, H. H.; Lee, Y. J.; Kim, S. K.; Ahn, S. *J. Phys. Chem. B.* **2005**, *109*, 13663−13667.
(28) Papageorgiou, N.; Athanassov, Y.; Armand, M.; Bonhôte, P.; Pettersson, H.; Azam, A.; Gratzel, M. *J. Electrochem. Soc.* **1996**, *143*, 3099−3108.
(29) Wang, P.; Zakeeruddin, S. M.; Moser, J.-E.; Humphry-Baker, R.; Grätzel, M. *J. Am. Chem. Soc.* **2004**, *126*, 7164−7165.
(30) Wang, P.; Zakeeruddin, S. M.; Moser, J.-E.; Grätzel, M. *J. Phys. Chem. B* **2003**, *107*, 13280−13285.
(31) Endres, F. *ChemPhysChem* **2002**, *3*, 144−154.
(32) Abbott, A. P.; Capper, G.; Davies, D. L.; Rasheed, R. K.; Tambyrajah, V. *Trans. Inst. Met. Finish.* **2001**, *79*, 204−206.
(33) El Abedin, S. Z.; Endres, F. *ACS Symp. Ser.* **2003**, *856*, 453−466.
(34) Endres, F.; Bukowski, M.; Hempelmann, R.; Natter, H. *Angew. Chem., Int. Ed.* **2003**, *42*, 3428−3430.
(35) Abbott, A. P.; Capper, G.; Swain, B. G.; Wheeler, D. A. *Trans. Inst. Met. Finish.* **2005**, *83*, 51−53.
(36) Wilkes, J. S.; Levisky, J. A.; Wilson, R. A.; Hussey, C. L. *Inorg. Chem.* **1982**, *21*, 1263−1264.
(37) Gale, R. J.; Gilbert, B.; Osteryoung, R. A. *Inorg. Chem.* **1978**, *17*, 2728−2729.
(38) Wilkes, J. S.; Zaworotko, M. J. *J. Chem. Soc., Chem. Commun.* **1992**, 965−967.
(39) Fuller, J.; Carlin, R. T.; Delong, H. C.; Haworth, D. *J. Chem. Soc., Chem. Commun.* **1994**, 299−300.
(40) Holbrey, J. D.; Seddon, K. R. *J. Chem. Soc., Dalton Trans.* **1999**, 2133−2139.
(41) Bonhôte, P.; Dias, A. P.; Papageorgiou, N.; Kalyanasundaram, K.; Grätzel, M. *Inorg. Chem.* **1996**, *35*, 1168−1178.
(42) Davis, J. H., Jr. *Chem. Lett.* **2004**, *33*, 1072−1077.
(43) Visser, A. E.; Swatloski, R. P.; Reichert, W. M.; Mayton, R.; Sheff, S.; Wierzbicki, A.; Davis, J. H.; Rogers, R. D. *Chem. Commun.* **2001**, 135−136.
(44) Visser, A. E.; Swatloski, R. P.; Reichert, W. M.; Mayton, R.; Sheff, S.; Wierzbicki, A.; Davis, J. H., Jr.; Rogers, R. D. *Environ. Sci. Technol.* **2002**, *36*, 2523−2529.
(45) Brasse, C. C.; Englert, U.; Salzer, A.; Waffenschmidt, H.; Wasserscheid, P. *Organometallics* **2000**, *19*, 3818−3823.
(46) Wasserscheid, P.; Waffenschmidt, H.; Machnitzki, P.; Kottsieper, K.; Selzer, O. *Chem. Commun.* **2001**, 451.
(47) Abbott, A. P.; Capper, G.; Davies, D. L.; Rasheed, R. K. *Chem.*−*Eur. J.* **2004**, *10*, 3769−3774.
(48) Abbott, A. P.; Capper, G.; Davies, D. L.; Munro, H. L.; Rasheed, R. K.; Tambyrajah, V. *Chem. Commun.* **2001**, 2010−2011.
(49) Abbott, A. P.; Capper, G.; Davies, D. L.; Rasheed, R. *Inorg. Chem.* **2004**, *43*, 3447−3452.
(50) Abbott, A. P.; Capper, G.; Davies, D. L.; Rasheed, R. K.; Tambyrajah, V. *Chem. Commun.* **2003**, 70−71.
(51) Abbott, A. P.; Capper, G.; Davies, D. L.; Rasheed, R. K.; Shikotra, P. *Inorg. Chem.* **2005**, *44*, 6497−6499.
(52) Abbott, A. P.; Capper, G.; Davies, D. L.; McKenzie, K. J.; Obi, S. U. *J. Chem. Eng. Data* **2006**, *51*, 1280−1282.
(53) Nyyssola, A.; Kerovuo, J.; Kaukinen, P.; von Weymarn, N.; Reinikainen, T. *J. Biol. Chem.* **2000**, *275*, 22196−22201.
(54) Becke, A. D. *J. Chem. Phys.* **1993**, *98*, 5648−5652.
(55) Stephens, P. J.; Devlin, F. J.; Chabalowski, C. F.; Frisch, M. J. *J. Phys. Chem.* **1994**, *98*, 11623−11627.
(56) Ahlrichs, R.; Bär, M.; Häser, M.; Horn, H.; Kölmel, C. *Chem. Phys. Lett.* **1989**, *162*, 165−169. For the current version, see http://www.turbomole.de.
(57) The Turbomole basis set library is available via an anonymous ftp, ftp://ftp.chemie.uni-karlsruhe.de/pub/basen.
(58) Boys, S. F.; Bernardi, F. *Mol. Phys.* **1970**, *19*, 553−566.
(59) van Duijnenveldt, F. B.; van Duijeveldt-van de Rijdt, J. G. C. M.; van Lenthe, J. H. *Chem. Rev.* **1994**, *94*, 1873−1885.
(60) Dunlap, B. I.; Connolly, J. W. D.; Sabin, J. R. *J. Chem. Phys.* **1979**, *71*, 3396−3402.
(61) Baerends, E. J.; Ellis, D. E.; Ros, P. *Chem. Phys.* **1973**, *2*, 41−51.
(62) Davidson, E. R. *J. Chem. Phys.* **1967**, *46*, 3320−3324.
(63) Schaftenaar, G.; Noordik, J. H. *J. Comput.-Aided Mol. Des.* **2000**, *14*, 123−134.
(64) Humphrey, W., Dalke, A. and Schulten, K., *J. Mol. Graphics* **1996**, *14*, 33−38.
(65) *Gaussview 3.0*; Gaussian, Inc.: Pittsburgh, PA, 2003.
(66) The CPMD consortium Web page can be accessed via http://www.cpmd.org/.
(67) Becke, A. D. *J. Chem. Phys.* **1993**, *98*, 5648−5652.
(68) Stephens, P. J.; Devlin, F. J.; Chabalowski, C. F.; Frisch, M. J. *J. Phys. Chem.* **1994**, *98*, 11623−11627.
(69) Troullier, N.; Martins, J. L. *Phys. Rev. B* **1991**, *43*, 1993−2006.
(70) Kleinman, L.; Bylander, D. M. *Phys. Rev. Lett.* **1982**, *48*, 1425−1428.
(71) Davidson, E. R. *J. Chem. Phys.* **1967**, *46*, 3320−3324.
(72) Roby, K. R. *Mol. Phys.* **1974**, *27*, 81−104.
(73) Pittois, S.; Van Roie, B.; Glorieux, C.; Thoen, J. *J. Chem. Phys.* **2004**, *121*, 1866−1872.
(74) Pittois, S.; Van Roie, B.; Glorieux, C.; Thoen, J. *J. Chem. Phys.* **2005**, *122*, 024504.
(75) Pittois, S. Ph.D. Thesis, Katholieke Universiteit Leuven, Belgium, 2004.
(76) *SAINT*, Manual Version 5/6.0; Bruker Analytical X-ray Systems Inc.: Madison, WI, 1997.
(77) *SHELXTL-PC*, Manual Version 5.1; Bruker Analytical X-ray Systems Inc.: Madison, WI, 1997.
(78) Weider, O. *Ber. Dtsch. Chem. Ges.* **1935**, *68B*, 263−267.
(79) Coronado, E.; Torment-Aliaga, A.; Gaita-Arino, A.; Giminez-Saiz, C.; Romero F. M.; Wernsdorfer, W. *Angew. Chem., Int. Ed.* **2004**, *43*, 6152−6156.
(80) Becke, A. D.; Edgecombe, K. E. *J. Chem. Phys.* **1990**, *92*, 5397−5403.
(81) Savin, A.; Becke, A. D.; Flad, J.; Nesper, R.; Preuss, H.; von Schnering, H. G. *Angew. Chem., Int. Ed. Engl.* **1991**, *30*, 409−412.
(82) Kohout, M.; Savin, A. *Int. J. Quantum Chem.* **1996**, *60*, 875−882.
(83) Kirchner, B.; Reiher, M. *J. Am. Chem. Soc.* **2002**, *124*, 6206−6215.
(84) Szafran, M.; Koput, J. *J. Mol. Struct.* **1997**, *404*, 91−104.
(85) Shikata, T. *J. Phys. Chem. A* **2002**, *106*, 7664−7670.
(86) Thar, J.; Kirchner, B. *J. Phys. Chem. A* **2006**, *110*, 4229−4237.
(87) Anisimov, M. A. *Critical phenomena in liquids and liquid crystals*; Gordon and Breach: Philadelphia, 1991.
(88) Chaikin, P. M.; Lubensky, T. C. *Principles of condensed matter*; Cambridge University Press: Cambridge, U.K., 1995.
(89) Zinn-Justin, J. *Phys. Rep.* **2001**, *344*, 159−178.
(90) Thoen, J.; Hamelin, J.; Bose, T. K. *Phys. Rev. E* **1996**, *53*, 6264−6270.
(91) Mensah-Brown, H.; Wakeham, W. A. *Int. J. Thermophys.* **1994**, *15*, 647−659.
(92) Mensah-Brown, H.; Wakeham, W. A. *Int. J. Thermophys.* **1995**, *16*, 237−244.
(93) Wagner, M.; Stanga, O.; Schröer, W. *Phys. Chem. Chem. Phys.* **2004**, *6*, 4421−44312004.
(94) Schröer, W. Criticality of ionic liquids in solution. In *Ionic soft matter. Modern trends and applications*; Henderson, D., Holovko, M., Trokhymchuk, A., Eds.; NATO Science Series II: Mathematics, Physics and Chemistry, Vol. 206; Springer: Berlin, 2005.
(95) Bird, M. J.; Lomer, T. R. *Acta Crystallogr., B* **1972**, *28*, 242−246.
(96) Doyle, A.; Felcman, J.; Gambardella, M. T. D.; Verani, C. N.; Tristao, M. L. B. *Polyhedron* **2000**, *19*, 2621−2627.
(97) Fischer, M. S.; Templeton, D. H.; Zalkin, A. *Acta Crystallogr., B* **1970**, *26*, 1392−1397.
(98) Rodriguez, V. H.; Paixao, J. A.; Costa, M. M. R. R.; Beja, A. M. *Acta Crystallogr., C* **2001**, *57*, 761−763.
(99) Ilczyszyn, M.; Godzisz, D.; Ilczyszyn, M. M. *J. Mol. Struct.* **2002**, *611*, 103−118.
(100) Rodrigues, V. H.; Paixao, J. A.; Costa M. M. R. R.; Beja, A. M. *Acta Crystallogr., C* **2001**, *57*, 213-215.
(101) Godzisz, D.; Ilczyszyn, M. M.; Ilczyszyn, M. *J. Mol. Struct.* **2002**, *606*, 123−137.
(102) Fujii, K.; Fujimori, T.; Takamuku, T.; Kanzaki, R.; Umebayashi, Y.; Ishiguro, S.-I. *J. Phys. Chem. B* **2006**, *110*, 8179−8183.
(103) Johansson, P.; Tegenfeldt, J.; Lindgren, J. *J. Phys. Chem. A* **2000**, *104*, 954−961.
(104) Canongia Lopes, J. N.; Padua, A. A. H. *J. Phys. Chem. B* **2004**, *108*, 16893−16898.
(105) Zhang, X. R.; Pugh, J. K.; Sukpirom, N.; Lerner, M. M. *Int. J. Inorg. Mater.* **2000**, *2*, 115−122.

(106) Herstedt, M.; Henderson, W. A.; Smirnov, M.; Ducasse, L.; Servant, L.; Talaga, D., Lassgues, J. C. *J. Mol. Struct.* **2006**, *783*, 145−156.

(107) Turner E. A.; Pye, C. C.; Singer, R. D. *J. Phys. Chem. A* **2003**, *107*, 2277−2288.

(108) Paulechka, Y. U.; Kabo, G. J.; Blokhin, A. V.; Vydrov, O. A.; Magee, J. W.; Frenkel, M. *J. Chem. Eng. Data* **2003**, *48*, 457−462.

(109) Katsyuba, S. A.; Dyson, P. J.; Vandyukova, E. E.; Chernova, A.; Vidis, A. *Helv. Chim. Acta* **2004**, *87*, 2556 2565.

(110) Heimer, N. E.; Del Sesto, R. E.; Carper, W. R. *Magn. Reson. Chem.* **2004**, *42*, 71−75.

(111) Liu, Z.; Huang, S.; Wang, W. *J. Phys. Chem. B* **2004**, *108*, 12978−12989.

(112) Tsuzuki, S.; Tokuda, H.; Hayamizu, K.; Watanabe, M. *J. Phys. Chem. B* **2005**, *109*, 16474−16481.

(113) Holbrey, J. D.; Reichert, M. W.; Rogers, R. D. *Dalton Trans.* **2004**, 2267−2271.

(114) Deetlefs, M.; Hardacre, C.; Nieuwenhuyzen, M.; Padua, A. A. H.; Sheppard, O.; Soper, A. K. *J. Phys. Chem. B*, in press.

(115) Kirchner, B. *J. Chem. Phys.* **2005**, *123*, 204116.

(116) Kirchner, B.; Hutter, J. *J. Chem. Phys.* **2004**, *121*, 5133−5142.

(117) Cammarata, L.; Kazarian, S. G.; Salter, P. A.; Welton, T. *Chem. Phys. Phys. Chem.* **2001**, *3*, 5192−5200.

(118) Köddermann, T.; Wertz, C.; Heintz, A.; Ludwig, R. *Angew. Chem., Int. Ed.* **2006**, *45*, 3697−3702.

(119) Price, W. D.; Jockusch, R. A.; Williams, E. R. *J. Am. Chem. Soc.* **1998**, *120*, 3474−3484.

(120) Crosthwaite, J. M.; Muldoon, M. J.; Aki, S. N. V. K.; Maginn, E. J.; Brennecke, J. F. *J. Phys. Chem. B* **2006**, *110*, 9354−9361.

(121) Scurto, A. M.; Aki, S. N. V. K.; Brennecke, J. F. *J. Am. Chem. Soc.* **2002**, *124*, 10276−10277.

(122) Aki, S. N. V. K.; Scurto, A. M.; Brennecke, J. F. *Ind. Eng. Chem. Res.*, in press.

(123) Scurto, A. M.; Aki, S. N. V. K., Brennecke, J. F. *Chem. Commun.* **2003**, 572−573.

(124) Suarez, P. A. Z.; Einloft, S.; Dullius, J. E. L.; de Souza, R. F.; Dupont, J. *J. Chim. Phys. Phys.-Chim. Biol.* **1998**, *95*, 1626−1639.

(125) Quagliano, J. V.; Kida, S.; Fujita, J. *J. Am. Chem. Soc.* **1962**, *84*, 724−729.

(126) Chen, X. M. Mak T. C. W. *Inorg. Chem.* **1994**, *33*, 2444−2447.

(127) Chen, X. M.; Mak, T. C. W. *Inorg. Chim. Acta* **1991**, *189*, 3−5.

(128) Chen, X. M.; Mak, T. C. W. *Polyhedron* **1991**, *10*, 273−276.

(129) Chen, X. M.; Mak, T. C. W. *Polyhedron* **1991**, *10*, 1723−1726.

(130) Chen, X. M.; Mak, T. C. W. *J. Chem. Soc., Dalton Trans.* **1991**, 1219−1222.

(131) Chen, X. M.; Wu, Y. L.; Yang, Y. Y.; Aubin, S. M. J.; Hendrickson, D. N. *Inorg. Chem.* **1998**, *37*, 6186−6191.